Thermal Conductivity of Fluids Containing Suspension of Nanometer-Sized Particles

by

Jack Jeinhao Ma

B.S., Mechanical Engineering (2003)
University of California, Berkeley

Submitted to the Department of Mechanical Engineering
in partial fulfillment of the requirements for the degree of

Master of Science in Mechanical Engineering

at the

MASSACHUSETTS INSTITUTE OF TECHNOLOGY

June 2006

Author .....
Department of Mechanical Engineering
May 12, 2006

Certified by .....
Gang Chen
Professor
Thesis Supervisor

Accepted by .....
Lallit Anand
Chairman, Department Committee on Graduate Students

Thermal Conductivity of Fluids Containing Suspension of Nanometer-Sized Particles

by

Jack Jeinhao Ma

Submitted to the Department of Mechanical Engineering on May 12, 2006, in partial fulfillment of the requirements for the degree of Master of Science in Mechanical Engineering

Abstract

Nanofluids, which are fluids containing suspension of nanometer-sized particles, have been reported to possess substantially higher thermal conductivity than their respective base fluids. This thesis reports on an experimental study of the effect of base fluid, particle size, particle volume concentration, and sonicating technique on the thermal conductivity enhancement of nanofluids. Thermal conductivity measurements for several combinations of nanocrystalline materials and base fluids were conducted with the transient hotwire technique. Results show that the thermal conductivity enhancement of nanofluids increases with particle volume concentration, with higher thermal conductivity enhancement observed for ethylene glycol than deionized water base fluids. However, most of the enhancement observed can be explained based on classical Maxwell-Garnett effective medium theory. Although ethylene glycol containing gold nanoparticles produces significantly higher enhancement in thermal conductivity over those predicted by the Maxwell-Garnett theory, Fourier transform analysis indicates that the anomalous enhancement in thermal conductivity observed with the gold-ethylene glycol nanofluids is due to the presence of water. Furthermore, results show that higher enhancement in thermal conductivity can be obtained by sonicating the aluminum

oxide-deionized water nanofluids with a more powerful sonicating tool prior to thermal conductivity measurement. This leaves room for future exploration in the effect of particle size and distribution on heat transfer in nanofluids.

Acknowledgments

This project could not have been completed without the support of many people. First, I would like to thank my research advisor, Professor Gang Chen, for his guidance throughout this project. Secondly, I would like to thank Dr. Jinbo Wang for his help on developing my transient hotwire apparatus. His former experience on thermal conductivity measurements of fluids made my experiment building process smooth and enjoyable. Also, I would like to thank people from Ford (Dustyn Sawall and Hiroko Ohtani), Professor Gareth McKinley, Jivtesh Garg, and Jeremy Gordon for their collaboration and valuable feedback. Finally, I would like to thank Ford-MIT Alliance for their financial support.

Table of Contents

List of Figures

Chapter 1: Introduction

1.1 Background

Thermal conductivity of heat transfer fluids plays a vital role in the development of high performance heat-exchange devices. Conventional fluids such as water and ethylene glycol are unable to meet the ever increasing demand for cooling in high energy applications such as automobile engines, lasers, and electronic chips due to their low thermal conductivity. Driven by industrial needs of high performance cooling, nanofluids which are suspensions of nanometer-sized particles in conventional fluids are currently being developed [1-5] This new class of fluids has garnered much interest from both academia and industry due to their enhanced thermal conductivity [6-7].

Numerous studies on the heat transfer properties of particle-liquid mixtures have been conducted in the past decades [8-10]. However, these early studies were limited to suspensions of millimeter- or micrometer-sized particles. The inherent problems with these relatively large particles are that the particles can quickly settle out of the solution, clog microchannels of small devices, and abrade surfaces due to the higher inertia of these particles. With the recent advances in nanocrystalline materials processing, these problems can be eliminated by reducing the size of suspended particles in a liquid to the nanoscale.

1.2 Experimental Investigation of Nanofluids

Since the emergence of nanotechnology and nanoscience, several processing methods have been developed to manufacture nanoparticles for scientific research and engineering applications [11-13]. The most common is inert gas condensation method [7]. In this method, a precursor material is first vaporized in a vacuum chamber. As the vaporized precursor material is brought in contact with an inert gas, it condenses into nanoparticles which then deposit on a cooled surface. Gleiter et al. showed that the resulting particle size distribution is determined by the evaporation rate of the precursor material, the inert gas pressure, and the evaporation temperature [14]. Currently, the inert gas condensation method is able to produce nanoparticles in large quantities [7].

Nanoparticles dispersed in a liquid tend to agglomerate and settle out of the solution after a certain period of time. Evidence shows that nanoparticles can be stabilized against agglomeration through either electrostatic repulsion or steric stabilization [3, 15]. Electrostatic repulsion results from the formation of an electrical double layer around the nanoparticles through the absorption of cations or anions in a liquid. The strength of this repulsive force is characterized by the zeta potential and is highly dependent on the pH of the liquid. Steric stabilization, on the other hand, results from absorption of surfactant groups around nanoparticles. The surfactant groups wrap around the nanoparticles with their chain structures to prevent the nanoparticles from further agglomeration towards bulk clusters. The capability to stabilize nanoparticle suspension allows further laboratory studies of thermal properties of nanofluids.

Numerous experimental investigations have been conducted to examine the effect of nanoparticle suspension in a base fluid on the effective thermal conductivity. Early experimental studies on the thermal conductivity of nanofluids focused on the colloidal suspension of oxide nanoparticles. Masuda et al. reported a 30% enhancement in thermal conductivity after adding ~4.3 vol. % of 13 nm aluminum oxide particles in water [1]. Zhou and Wang et al. found that the thermal conductivity of water can be increased by ~17% with the addition of only ~0.4 vol. % of 50 nm copper oxide particles [16]. Other research groups have demonstrated promising results from dispersion of metallic nanoparticles such as copper and gold. Eastman et al. observed a ~40% enhancement in thermal conductivity with ethylene glycol containing ~0.3 vol. % of 10 nm copper particles [6]. Patel et al. reported ~7% enhancement when 0.011 vol. % of gold nanoparticles were dispersed in toluene [17]. These results show enhancement in thermal conductivity significantly above that predicted by the effective medium theories.

1.3 Theoretical Investigation of Nanofluids

Theoretical modeling of heat transfer properties of particle suspension in a medium began in the late nineteenth century when Maxwell's theoretical work was first proposed [18]. In his work, Maxwell developed a model to predict the effective thermal conductivity of composites containing dispersion of spherical particles. The radii of the particles were assumed to be small compared to the inter-particle distances so that interference among particles can be avoided. This assumption is valid when the volume fraction of particles is limited to a small amount. Maxwell's model showed that thermal conductivity of a base

medium can be enhanced by adding spherical particles of high thermal conductivity, and the effective thermal conductivity of particle-base medium composite increases with increased particle volume fraction [18]. Although Maxwell's model may provide a good approximation for large particle suspensions, it cannot explain the thermal transport phenomena in nanometer-sized particle suspensions because it did not include the boundary thermal resistance.

Heat transfer in a nanofluid can be modeled as heat flow through a solid-liquid composite system. It has been recognized that in a composite system, the temperature drop across the interface between materials may be appreciable [19]. This temperature difference is attributed to the existence of a boundary thermal resistance, which is due to imperfect contact (mechanically or chemically) between dissimilar materials and a mismatch in the coefficient of thermal expansion [20]. Boundary thermal resistance is smaller at a solid-liquid interface than at a solid-solid interface due to better contact between liquid and solid. A simple parameter to characterize the importance of the boundary thermal resistance in a solid-liquid mixture is thermal resistance thickness defined as the width of the liquid layer over which there exists the same temperature drop as that across the solid-liquid interface [21]. The thermal resistance thickness of a liquid containing large size particles is small, but as the dimension of the particles approaches the nanoscale, this thickness can become comparable to the particle size and inter-particle distance. In this case, the boundary thermal resistance can no longer be neglected in theoretical models of heat transfer in a solid-liquid mixture.

Experimental work conducted by Hatta and Power [22-23] on the thermal diffusivity of fiber-reinforced glass ceramic and sodium borosilicate glass matrix containing dispersion of spherical nickel indicated that the effective thermal conductivity of composites can be

affected by the boundary thermal resistance at the interface between the matrix and the dispersed fibers or particles. In view of the significance of boundary thermal resistance in a composite system, Hasselman and Johnson modified Maxwell's theory to include the effect of boundary thermal resistance and particle size [20]. The resulting form of effective thermal conductivity of a particle-liquid mixture is given by:

$$\frac{k_{eff}}{k_m} = \frac{k_p(1 + 2\alpha) + 2k_m + 2\phi\,[k_p(1 - \alpha) - k_m]}{k_p(1 + 2\alpha) + 2k_m - \phi\,[k_p(1 - \alpha) - k_m]} \qquad (1.1)$$

where k_m and k_p are the thermal conductivity of liquid and particle respectively, ϕ is the particle volume fraction, and $\alpha = 2R_b k_m/d$ where R_b is the boundary thermal resistance and d is the particle diameter. In the absence of boundary thermal resistance, $R_b = 0$, Eq. (1.1) reduces to Maxwell's model [18].

Several mechanisms that may contribute to the enhanced thermal conductivity of nanofluids have been proposed by the nanofluid research community. These include liquid layering at liquid-particle interface, Brownian motion of nanoparticles, and nanoparticle clustering. However, none of these mechanisms have adequately explained the anomalous enhancement in nanofluid thermal conductivity [24-26]. Hence, the principal objective of this thesis is to explore the mechanisms of heat transfer enhancement in nanofluids through experimental investigations.

This thesis is organized as follows. Chapter 2 discusses the experimental method and technique used to determine thermal conductivity of nanofluids. Chapter 3 describes manufacturers' specification of the nanofluid samples (i.e. particle size, particle volume concentration...etc) under current investigation, as well as how the samples were prepared

before thermal conductivity measurements. Results of thermal conductivity enhancement of nanofluids over their respective base fluids were discussed in Chapter 4. Chapter 5 summarizes the research and discusses future work of nanofluids study.

Chapter 2: Experimental Method and Technique

2.1 Determination of Liquid Thermal Conductivity

Two experimental methods are commonly used for determining the thermal conductivity of liquids: the steady-state method and the transient hotwire method. The steady-state method typically involves applying a heat flux to create a steady-state temperature difference across a liquid layer, whereas the transient hotwire approach involves generating a temperature variation of a metallic wire suspended in a liquid.

Wang and Xu et al. used a steady-state parallel-plate method, originally designed by Challoner and Powell [27], to measure the thermal conductivity of aluminum oxide and copper oxide dispersion in water, vacuum pump fluid, engine oil, and ethylene glycol [28]. A schematic of the experimental apparatus is shown in Figure 2.1. The liquid sample is located in the volume between two parallel round copper plates separated by three glass spacers of known thickness and thermal conductivity. The upper copper plate is surrounded by an aluminum cell. Thermocouples are used to measure temperatures of the bottom surface of the upper copper plate and the top surface of the lower copper plate. During the experiment, heater 1, embedded on the top copper plate, generates a heat flux from the upper copper plate through the liquid sample to the lower copper plate. Heaters 2 and 3 are used to equalize temperature of the aluminum cell to that of the upper copper plate. The temperature of the lower copper plate is maintained uniform by heater 4. With the known heat flux and temperature difference across the region between the two parallel copper plates, the effective thermal conductivity of the liquid-glass composite can be calculated from one-dimensional heat conduction equation:

$$k_c = \frac{\dot{q} L_g}{A \Delta T} \tag{2.1}$$

where $\dot{q}$ is the power of Heater 1, L_g is the thickness of the glass spacer, A is the area of the top copper plate orthogonal to the direction of heat flow, and ΔT is the temperature difference between the two copper plates. The thermal conductivity of the liquid can then be obtained from the effective thermal conductivity of liquid-glass composite using the following relation

$$k_l = \frac{k_c A - k_g A_g}{A - A_g} \tag{2.2}$$

where k_c is the thermal conductivity of the liquid-glass composite, k_g is the thermal conductivity of the glass spacer, and A_g is the area of the glass spacer normal to the direction of heat flow. Calibration experiments showed that the absolute error for the thermal conductivity of deionized (DI) water and ethylene glycol obtained with this steady-state parallel-plate method is less than $\pm 3\%$ [28]. In applying this method for the determination of liquid thermal conductivity, one must pay special attention to the temperature difference between the inside wall of aluminum cell and the upper copper plate. The existence of this temperature difference results in natural convection and radiation losses from the top copper plate, which reduce the amount of heat flux between the two copper plates.

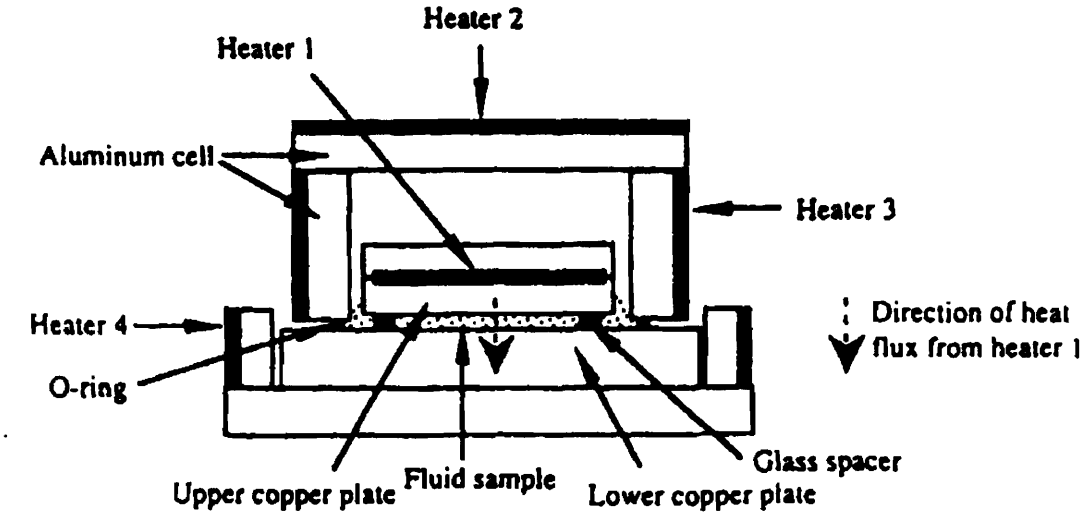

Figure 2.1 Experimental Apparatus for Steady-State Parallel-Plate Method [28]

Transient hotwire method, on the other hand, is currently the most commonly used method for determining the thermal conductivity of fluids [29-30]. It is called transient in the sense that the electric power is applied abruptly to a thin metallic wire surrounded by a fluid. The applied electric power results in joule heating and the subsequent temperature rise of the wire. This temperature variation of the wire as a function of time is strongly dependent on the heat transfer properties of the surrounding fluid, and it can be used to determine the thermal conductivity of a fluid. The most advantageous feature of the transient hotwire method is that it can experimentally eliminate error caused by natural convection [29]. Despite its high degree of accuracy, transient hotwire method cannot be used to measure the thermal conductivity of an electrically conducting fluid since significant leakage of electrical current can occur from the metallic wire to the surrounding fluid. However, this limitation can be overcome by using a metallic wire coated with a thin electrical insulation layer.

As opposed to the steady-state method which may takes hours for the system to reach steady-state, the duration of the transient hotwire method lasts only a few seconds. Also, elimination of natural convection and radiation losses with the transient hotwire method greatly simplifies experimental procedures. Hence, current experiment uses transient hotwire approach to measure liquid thermal conductivity.

2.2 Transient Hotwire Method

There are several assumptions made in the transient hotwire method. First, the wire is infinitely long and is surrounded by an infinite medium whose thermal conductivity is to be measured. Secondly, the wire is a perfect thermal conductor (i.e. infinite thermal conductivity) so that the temperature distribution within the wire can be treated as uniform. Finally, the wire loses heat radially through conduction alone to the surrounding medium.

There are three regions of conduction heat transfer from the wire to the surrounding fluid. Region 1 is the bare metallic wire, region 2 is the electrical insulation layer, and region 3 is the surrounding fluid (see Figure 2.2). The governing Fourier equation in the cylindrical coordinates in each of these three regions is:

$$\frac{\partial^2 \Delta T_1}{\partial r^2} + \frac{1}{r}\frac{\partial \Delta T_1}{\partial r} - \frac{1}{\kappa_1}\frac{\partial \Delta T_1}{\partial t} = -\frac{q}{\pi r_1^2 \lambda_1} \qquad for \quad 0 \le r \le r_1 \qquad (2.3)$$

$$\frac{\partial^2 \Delta T_2}{\partial r^2} + \frac{1}{r}\frac{\partial \Delta T_2}{\partial r} - \frac{1}{\kappa_2}\frac{\partial \Delta T_2}{\partial t} = 0 \qquad for \quad r_1 \le r \le r_0 \qquad (2.4)$$

$$\frac{\partial^2 \Delta T_3}{\partial r^2} + \frac{1}{r}\frac{\partial \Delta T_3}{\partial r} - \frac{1}{\kappa_3}\frac{\partial \Delta T_3}{\partial t} = 0 \qquad for \quad r_o \le r \qquad (2.5)$$

where r_1 is the radius of metallic wire, r_0 is the overall radius of coated wire, κ is the thermal diffusivity, λ is the thermal conductivity, and q is the heat generation per unit length of wire.

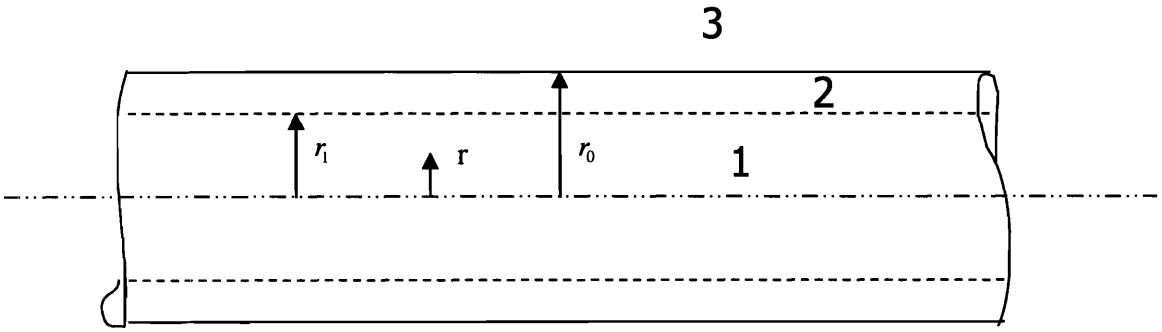

Figure 2.2 The Coordinate System of an Insulated Wire Immersed in a Liquid

Since there is no current passing through region 2 and 3 (see Figure 2.2), these two regions do not have the heat generation term in their corresponding Fourier equations (see Eq. (2.4) and Eq. (2.5)). The imposed initial and boundary conditions for this conduction problem are:

$$\Delta T_1 = \Delta T_2 = \Delta T_3 = 0 \qquad t \le 0 \qquad (2.6)$$

$$\lambda_1 \frac{\partial \Delta T_1}{\partial r} = \lambda_2 \frac{\partial \Delta T_2}{\partial r} \qquad r = r_1 \qquad (2.7)$$

$$\Delta T_1 = \Delta T_2 \qquad r = r_1 \qquad (2.8)$$

$$\lambda_2 \frac{\partial \Delta T_2}{\partial r} = \lambda_3 \frac{\partial \Delta T_3}{\partial r} \qquad r = r_0 \qquad (2.9)$$

$$\Delta T_2 = \Delta T_3 \qquad r = r_0 \qquad (2.10)$$

$$\Delta T_3 = 0 \qquad r \to \infty \qquad (2.11)$$

$$\frac{\partial \Delta T_1}{\partial r} = 0 \qquad r \to 0 \qquad (2.12)$$

Nagasaka et al. has derived an analytical expression for the solution of temperature distribution in region 1 using the previously stated initial and boundary conditions [29]. Since the transient hotwire method assumes that the wire has uniform temperature, an integral average along the radial coordinates is applied to the solution of temperature distribution $\Delta T_1(r, t)$. The resulting form of $\overline{\Delta T_1}(t)$ is given by:

$$\overline{\Delta T_1}(t) = \int_0^{r_1} \Delta T_1(r,t) \frac{2\pi r dr}{\pi r_1^2} = \frac{q}{4\pi\lambda_3}\left[\ln t + A + \frac{1}{t}(B \ln t + C)\right] \qquad (2.13)$$

where A, B , and C are constant terms involving the geometry of wire, the thermal diffusivity of region 1, 2, and 3, and the thermal conductivity of region 2 and 3.

If $\frac{1}{t}(B\ln t + C)$ is much less than the constant term A, which is the case for a wire with diameter in the microscale, there exists a linear relationship between $\overline{\Delta T_1}$ and time in logarithmic scale:

$$\overline{\Delta T_1} = \frac{q}{4\pi\lambda_3}[\ln t + A] \tag{2.14}$$

The slope of the line $\frac{d\overline{\Delta T_1}}{d\ln t}$ is given by $\frac{q}{4\pi\lambda_3}$, and therefore, the thermal conductivity of a fluid can be determined from

$$\lambda_3 = \frac{q}{4\pi} \Big/ \frac{d\overline{\Delta T_1}}{d\ln t} \tag{2.15}$$

2.3 Experimental Apparatus and Measurement Technique

Figure 2.3 shows the schematic of an electrical circuit for measuring the thermal conductivity of fluids. The change of hotwire temperature is measured by a Wheatstone bridge. Two arms of the bridge consist of two precision resistors. Each precision resistor has a resistance value of 40.13 kΩ and a temperature coefficient of resistance of 5 ppm/^{0}C. The other two arms of the bridge consist of the hotwire cell and a 100 Ω potentiometer with the temperature coefficient of resistance of 20 ppm/^{0}C. The voltage imbalance across the bridge as a function time is recorded by a data acquisition system.

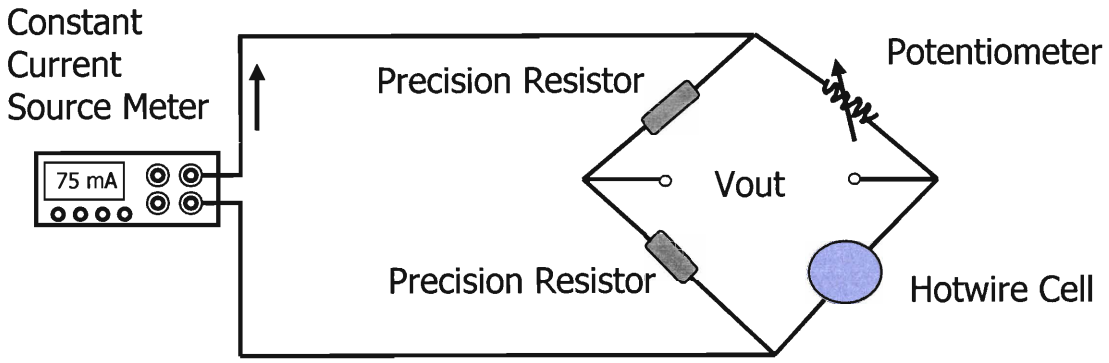

Figure 2.3 Schematic of Electrical Circuit

The hotwire cell contains an Isonel-coated platinum wire suspended horizontally in a fluid (see Figure 2.4). The wire is approximately 15 cm long and was soldered to copper/brass electrodes at both ends. The wire core diameter is 25 μm and the insulation layer has a thickness of 1.5 μm. To eliminate leakage of electrical current from the electrodes to the surrounding fluid, three layers of electrically insulating epoxy were applied to the surface of electrodes.

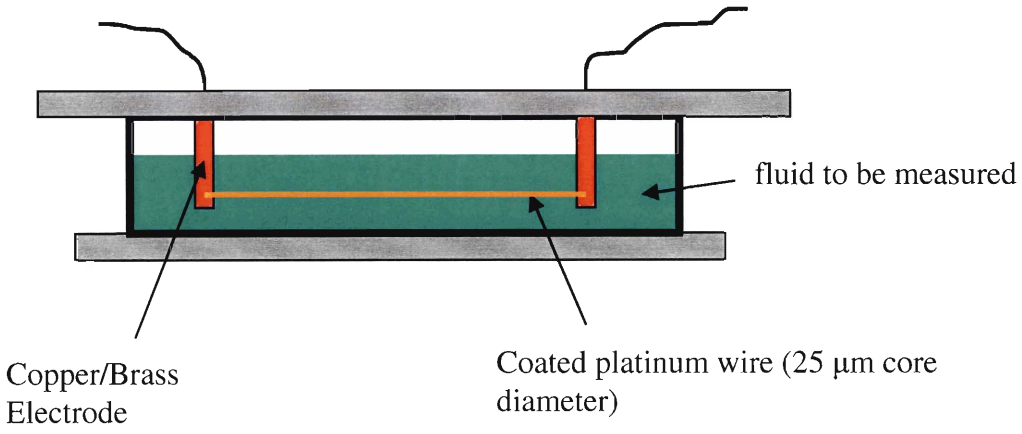

2.4 Schematic of Hotwire Cell

Figure 2.5 shows a photograph of the transient hotwire apparatus. To measure thermal conductivity, a fluid was first placed into the hotwire cell. Then, the potentiometer was adjusted until the voltage imbalance across the bridge was reduced to ~10 μV. After the bridge was initially balanced, the resistances of the hotwire cell and potentiometer were measured with a Digital Multimeters (DMM's) using four-wire method. Then, a constant current of 75 mA was applied to the bridge, and the voltage imbalance across the bridge in the range of 1 mV was recorded as a function of time. The duration of data acquisition was 2 seconds. Finally, signal analysis was performed to convert the bridge output signal to the thermal conductivity of a fluid (see Section 2.4).

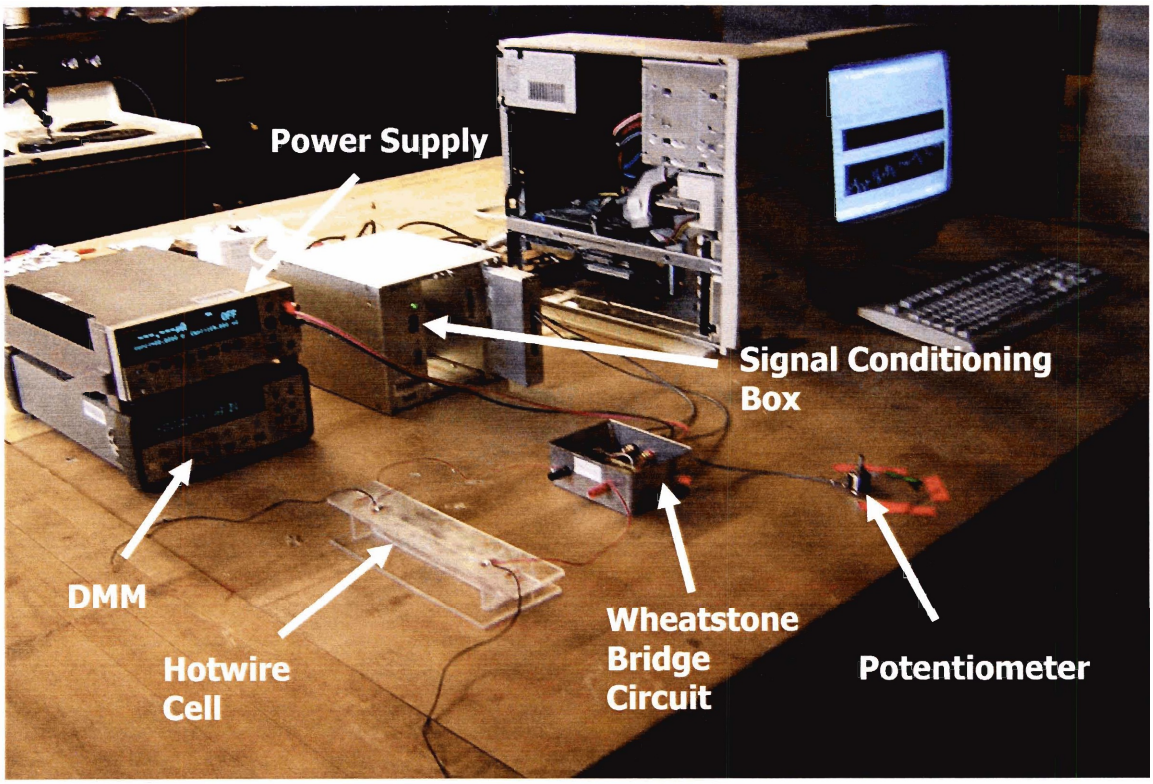

Figure 2.5 Transient Hotwire Apparatus

2.4 Signal Analysis for the Transient Hotwire Experiment

Wheatstone bridge is commonly used for high-accuracy resistance measurement. The output from the bridge is often directly connected to a high-impedance device such as an electronic voltmeter to determine the magnitude of bridge imbalance. Figure 2.6 shows a schematic for the Wheatstone bridge circuit used in the current transient hotwire experiment. R_1 and R_2 are the precision resistors with the same resistance value, R_3 is a 100 Ω potentiometer, R_w is the resistance of the hotwire, and Rp is the parasitic resistance associated with the hotwire cell. A constant current is applied to the bridge to produce voltage output due to bridge imbalance.

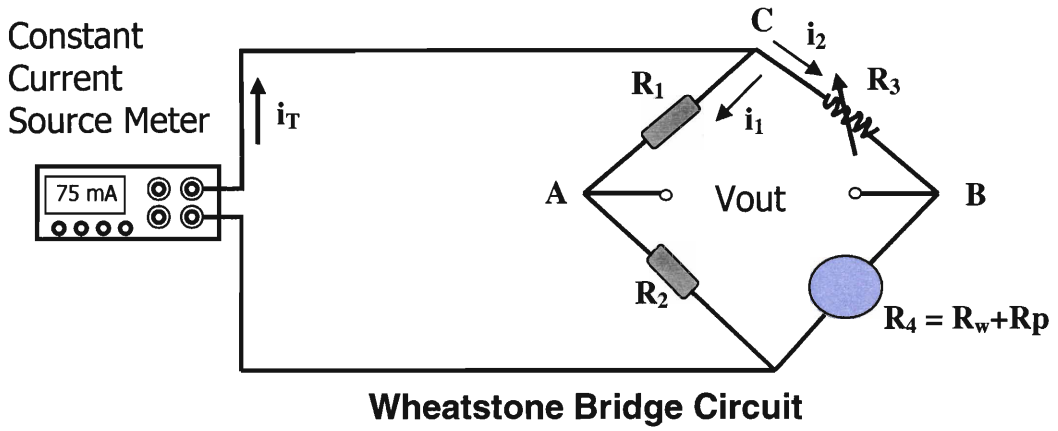

Figure 2.6 Wheatstone Bridge Circuit

From Figure 2.6, it can be seen that the bridge output is the difference between the voltage at point A and point B.

$$V_{out} = V_A - V_B \tag{2.16}$$

Using the voltage divider relation, V_{out} can be written as

$$V_{out} = V_{in}\left[\frac{R_W + R_p}{R_3 + R_w + R_p} - \frac{R_2}{R_1 + R_2}\right] \tag{2.17}$$

Let $R_W + R_p = R_4$ and substitute into Eq. (2.17)

$$\Rightarrow V_{out} = V_{in}\left[\frac{R_4}{R_3 + R_4} - \frac{R_2}{R_1 + R_2}\right]$$

$$= V_{in}\left[\frac{R_4R_1 - R_2R_3}{(R_1 + R_2)(R_3 + R_4)}\right] \tag{2.18}$$

Apply Kirchoff's current law at point C, and it gives

$$\begin{aligned} i_T &= i_1 + i_2 \\ &= \frac{V_{in}}{R_1 + R_2} + \frac{V_{in}}{R_3 + R_4} \\ &= V_{in}\left[\frac{R_1 + R_2 + R_3 + R_4}{(R_1 + R_2)(R_3 + R_4)}\right] \end{aligned} \tag{2.19}$$

Eq. (2.19) can be rearranged to give

$$V_{in} = i_T\left[\frac{(R_1 + R_2)(R_3 + R_4)}{(R_1 + R_2 + R_3 + R_4)}\right] \tag{2.20}$$

Substitute Eq. (2.20) into Eq. (2.18)

$$\begin{aligned} \Rightarrow V_{out} &= i_T\left[\frac{(R_1 + R_2)(R_3 + R_4)}{(R_1 + R_2 + R_3 + R_4)}\right]\left[\frac{R_4R_1 - R_2R_3}{(R_1 + R_2)(R_3 + R_4)}\right] \\ &= i_T\left[\frac{R_4R_1 - R_2R_3}{(R_1 + R_2 + R_3 + R_4)}\right] \\ &= i_T\left[\frac{(R_w + R_p)R_1 - R_2R_3}{(R_1 + R_2 + R_3 + R_w + R_p)}\right] \end{aligned}$$

If R_w changes by ΔR_w,

$$\Rightarrow V_{out} + \Delta V_{out} = i_T\left[\frac{(R_w + \Delta R_w + R_p)R_1 - R_2R_3}{(R_1 + R_2 + R_3 + R_w + \Delta R_w + R_p)}\right]$$

Assume the bridge is initially balanced, then $V_{out} = 0$, and let $R_1 = R_2 = R$

$$\Rightarrow \Delta V_{out} = i_T \left[\frac{(R_w + \Delta R_w + R_p)R - R R_3}{(R + R + R_3 + R_w + \Delta R_w + R_p)} \right]$$

$$\Rightarrow \Delta V_{out} = i_T \left[\frac{(R_w + R_p - R_3)R + \Delta R_w R}{(2R + R_3 + R_w + \Delta R_w + R_p)} \right] \qquad (2.21)$$

Eq. (2.21) can be rearranged to give

$$\Delta R_w = \left[\frac{(R_w + R_p - R_3)R - (2R + R_3 + R_w + R_p)\frac{\Delta V_{out}}{i_T}}{\frac{\Delta V_{out}}{i_T} - R} \right]$$

The change of hotwire temperature can be obtained from ΔR_w and the temperature coefficient of resistance of hotwire α, and it gives

$$\Delta T_w = \frac{\Delta R_w}{R_w(\alpha)} \qquad (2.22)$$

2.5 System Calibration

The coated platinum wire needed to be calibrated to obtain its temperature coefficient of resistance (TCR) defined as the change of resistance of a material per degree change of temperature. The calibration was done by measuring the resistance of the coated platinum wire when the wire was immersed in water at different temperatures. The wire resistance versus temperature is plotted in Figure 2.7. Results show that TCR of the coated platinum wire, which is $\frac{dR}{dT}$ divided by the resistance of the wire at room temperature (~25 °C), is 0.003359 $\Omega/(\Omega\,\mathrm{K})$. The published value of TCR for platinum wire, however, is 0.0039 $\Omega/(\Omega\,\mathrm{K})$ [31].

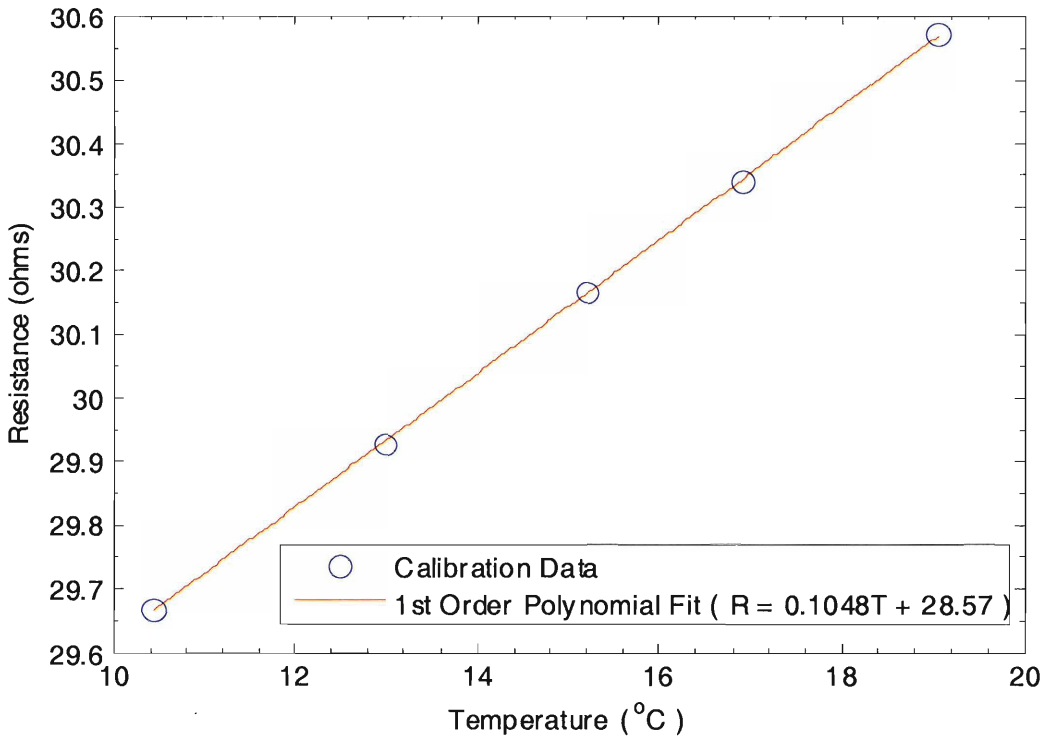

Figure 2.7 Hotwire Temperature Coefficient of Resistance Calibration

To establish the reliability of thermal conductivity measurement, calibration experiments were performed for DI water and ethylene glycol at room temperature (~25 °C). Figure 2.8 plots the change of temperature of the coated platinum wire as a function of time for both DI water and ethylene glycol. As seen in Figure 2.8, the change of wire temperature in both liquids increases with time in logarithmic scale. The change of wire temperature in the case of ethylene glycol is higher than that of DI water, and this is attributed to the fact that ethylene glycol has a lower thermal conductivity. Although Figure 2.8 shows ΔT vs. ln(time) in a full time scale, the slope of the curve is only obtained from the data range between 0.1 and 1 second. This is because at short time scale, internal heat conduction inside the wire is dominating, and data cannot be used, whereas at long time scale, convection sets in and cause the slope of ΔT vs. ln(time) curve to diverge from linearity (see Figure 2.8).

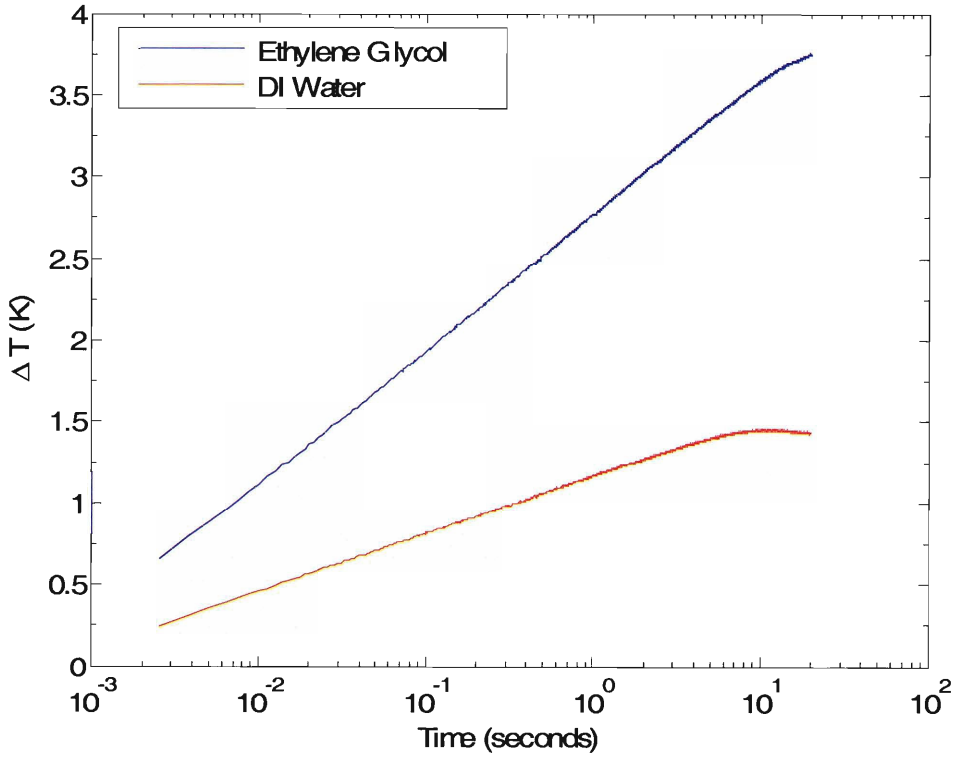

Figure 2.8 Calibration Data for DI Water and Ethylene Glycol at Room Temperature

From the slope of ΔT vs. ln(time), the thermal conductivity of DI water and ethylene glycol can be calculated using Eq. (2.15), and the results are compared with the literature values (see Table 2.1). Table 2.1 shows that at room temperature, the measured thermal conductivity of both liquids is lower than the literature values by less than 2%. The uncertainty shown in the measured thermal conductivity was obtained from the standard deviation of eight data points.

Table 2.1 Measured Thermal Conductivity vs. Literature Values

Fluid	Measured Thermal Conductivity (W/mK)	Literature Value (W/mK)	Error (%)
Deionized Water (~25 °C)	0.599 ± 0.002 ($\pm 1\sigma$)	0.608	1.5
Ethylene Glycol (~25 °C)	0.248 ± 0.001 ($\pm 1\sigma$)	0.252	1.6

2.6 The Effect of Thermophoresis and Electrophoresis on Transient Hotwire Measurement

As an electrical current is applied to the hotwire, a temperature gradient and an electric field are generated in the vicinity of hotwire. Hence, thermophoresis and electrophoresis may have a considerable impact on the thermal conductivity measurement of a nanofluid using transient hotwire technique [32-33]. Thermophoresis is the force exerted on particles due to the presence of a temperature gradient. It is a result of force imbalance associated with molecular collision from the colder and hotter regions. Electrophoresis, on the other hand, is the force exerted on the charged particles under the influence of an electric field. It has been known that particles are charged when they are suspended in a liquid. These charges can be obtained either from the absorption of ions in a liquid or from the ionization of chemical groups in the surface of particles.

To study the effect of thermophoresis and electrophoresis on the thermal conductivity measurement, heating power and hotwire diameter were varied to produce different temperature gradient and strength of electric field in the vicinity of the hotwire. The nanofluid used for the thermophoresis and electrophoresis experiments is alumina in ethylene glycol with particle diameter of 35 nm and particle volume concentration of 5%. The results are shown in Figure 2.9 and Figure 2.10. As illustrated in these two figures, the thermal conductivity enhancement is independent on heating power and hotwire geometry. This indicates that the effect of thermophoresis and electrophoresis on heat transfer characteristic in a nanofluid cannot be observed experimentally.

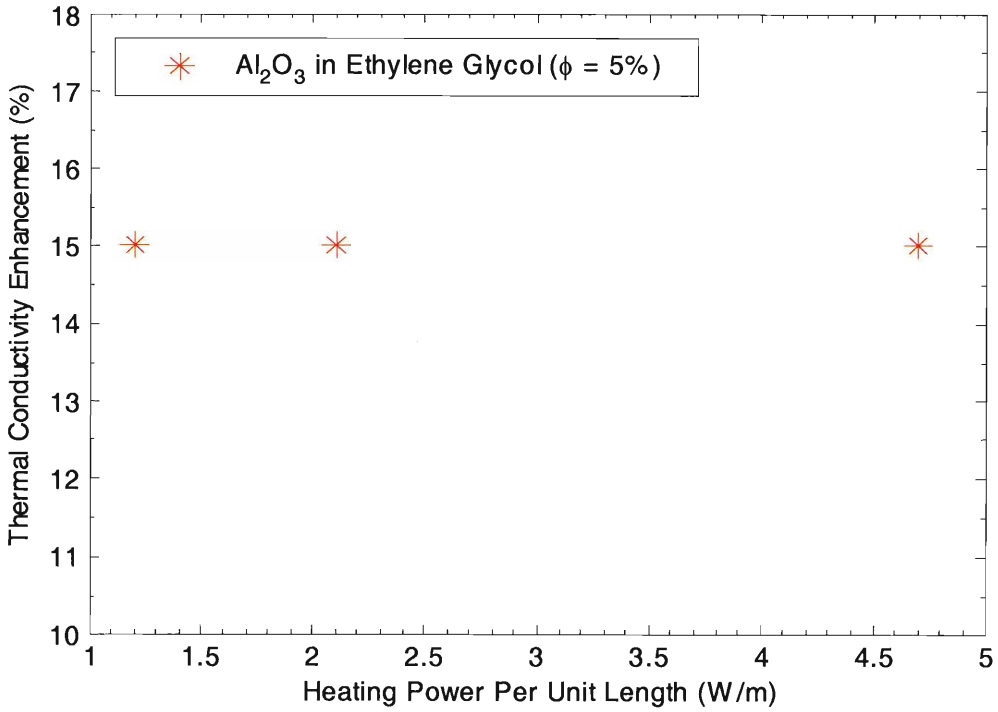

Figure 2.9 The Effect of Heating Power on the Thermal Conductivity Enhancement

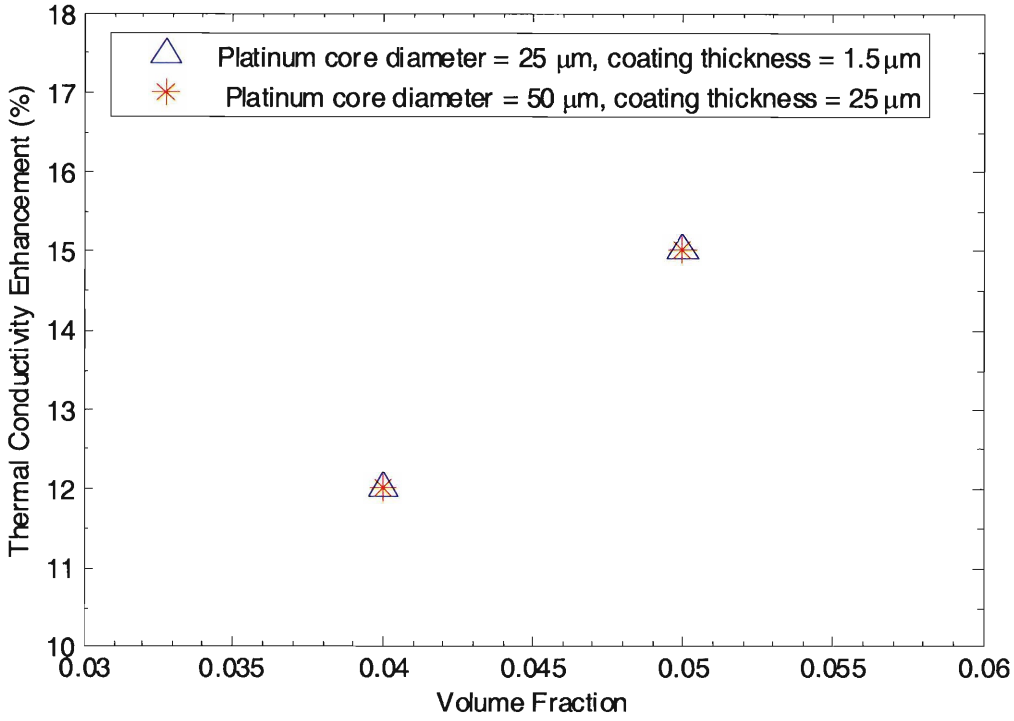

Figure 2.10 The Effect of Hotwire Diameter on the Thermal Conductivity Enhancement

2.7 Attenuated Total Reflection-Fourier Transform Infrared Spectroscopy (ATR-FTIR)

It is of interest to confirm that the composition of a fluid sample is consistent with the manufacturer's claim. This can be done by using Fourier Transform Infrared Spectroscopy (FTIR), which is an analytical technique for material analysis. FTIR can be used to identify types of chemical bonds or functional groups in an unknown solid, liquid, or gas. One application of FTIR involves detecting contaminants or dissolved species in liquids.

Attenuated total reflection (ATR) is a recently developed FTIR sampling technique. ATR technique allows analysis of a solid or liquid sample with little or no sample preparation. The sample is simply placed in contact with the top face of an ATR crystal, which is often referred to as an internal reflection element. ATR technique works well with samples that are either too thick or too absorbing for standard transmission analysis.

To obtain ATR spectra of a liquid sample, a droplet of liquid is placed in direct contact with an ATR crystal of high refractive index. Then, an infrared beam is directed into the crystal at a certain angle such that total internal reflection occurs along the interface between the crystal and the sample (see Figure 2.11). The infrared beam reflects from this interface and creates an evanescent wave that extends orthogonally beyond the crystal into the sample. Typically, the evanescent wave penetrates into the sample in the order of a few microns. As some of its energy is absorbed by the sample at certain absorption frequencies, the evanescent wave becomes attenuated. This attenuated evanescent wave is then passed back to the infrared beam, which leaves the crystal and enters a detector in the FTIR spectrometer.

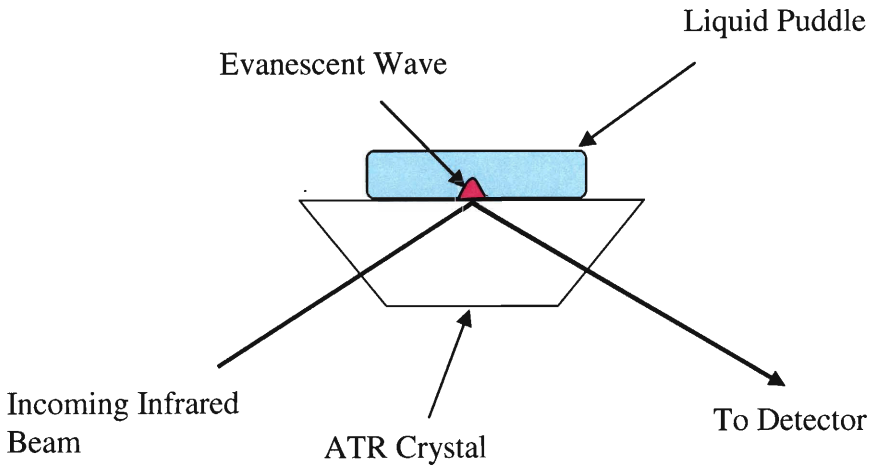

Figure 2.11 Single Reflection ATR System

Chapter 3: Sample Description and Preparation

3.1 Sample Description

The nanofluids under current investigation can be divided into two groups, which are DI water- and ethylene glycol-based nanofluids. Both groups consist of suspension of aluminum oxide and gold nanoparticles (see Table 3.1 and Table 3.2). The particle size shown in these two tables refers to the size of the particles prior to their dispersion in the base fluids. To enhance colloidal stability, commercially available surfactants such as pyridine and sodium dodecylbenzenesulfonate are used in some nanofluid samples. Pyridine is a clear liquid, whereas sodium dodecylbenzenesulfonate is solid and is soluble in most solvents. All nanofluid samples were prepared by a two-step method, in which the nanoparticles were produced first, followed by dispersion of nanoparticles in the base fluids.

Table 3.1 DI Water-Based Nanofluids

Suspended Particles	Particle Size	Particle Volume Concentration(as received from manufacturer)	Surfactant	Manufacturer
Aluminum Oxide	47 nm	~8%	without Surfactant	Nanophase Technologies
Gold	5, 15, and 30 nm	~0.27%	without Surfactant	Meliorum Technology
Gold	15 nm	~0.27%	Pyridine	Meliorum Technology

Table 3.2 Ethylene Glycol-Based Nanofluids

Suspended Particles	Particle Size	Particle Volume Concentration(as received from manufacturer)	Surfactant	Manufacturer
Aluminum Oxide	35 nm	~5%	NaDBS*	Meliorum Technology
Gold	5, 15, and 30 nm	~0.3%	without surfactant	Meliorum Technology
Gold	15 nm	~0.3%	Pyridine	Meliorum Technology

*NaDBS – sodium dodecylbenzenesulfonate

3.2 Sample Preparation

3.2.1 Sonication

Particles in nanofluids tend to agglomerate to form clusters, which will eventually become unstable and settle out of the solutions. Some energy is required to break clusters into smaller constituents. In this experiment, two techniques were employed to break nanoparticle clusters in nanofluids. The first technique, also the primary technique used in this experiment, involved immersing the nanofluid samples in an ultrasonic cleaner capable of generating ultrasonic pulses of 70 W at 42 kHz (see Figure 3.1). Before conducting thermal conductivity measurements, nanofluid samples were sonicated in the ultrasonic cleaner for ~4 hours.

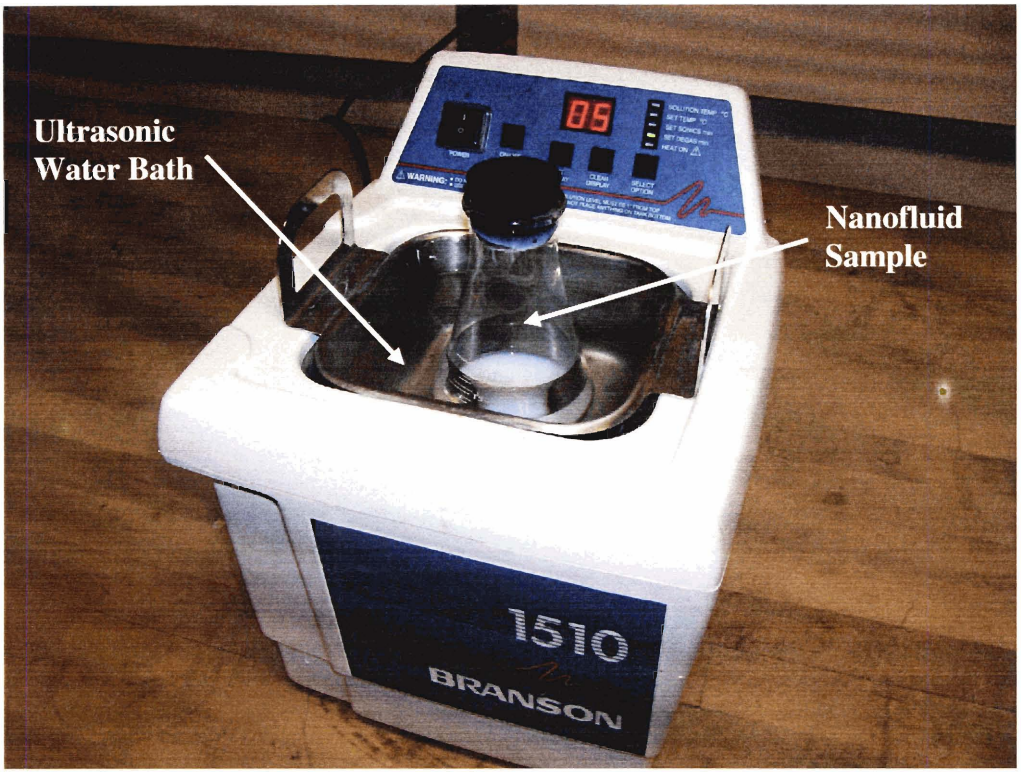

Figure 3.1 Ultrasonic Cleaner Setup

The second technique of separating aggregates into smaller constituents involved using an ultrasonic probe, which is able to generate a power output of 750 W at 20 kHz. The probe was immersed ~5 cm into a nanofluid sample, and was operated on pulsed mode (i.e. the probe was turned on for 2 seconds, followed by 1 second of inactivity) to provide mixing by repeatedly allowing the sample to settle back under the probe after each burst (see Figure 3.2). The ultrasonic probe was programmed to continue sonicating the sample until ~16000 J of ultrasonic energy was delivered to the sample.

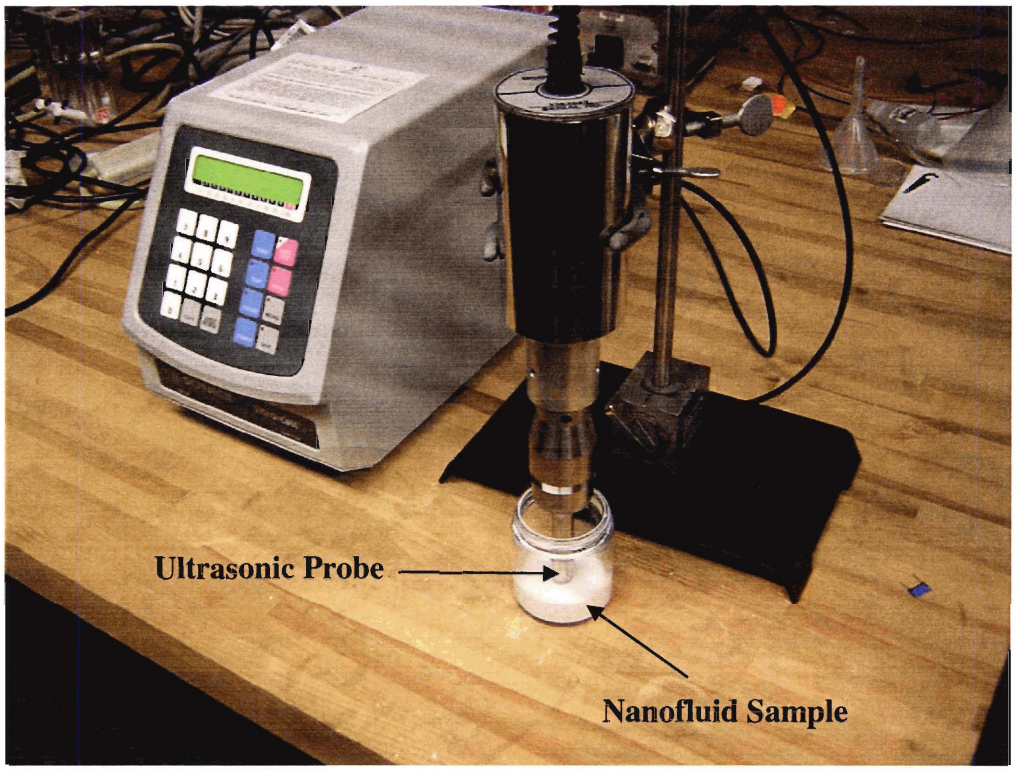

Figure 3.2 Ultrasonic Probe Setup

3.2.2 Diluting Procedure

A diluting procedure was followed to dilute a nanofluid to a lower particle concentration. First of all, a nanofluid sample was sonicated in an ultrasonic cleaner. After sonication, the sample was shaken rigorously to ensure that colloidal particles were uniformly distributed in the solution. Then, the amount of nanofluid required for dilution is withdrawn by a pipette. Finally, the diluting solvent was added to the withdrawn nanofluid to dilute the original sample to the particle volume concentration of interest. The diluting solvents used are ethylene glycol and DI Water, and their properties are shown in Table 3.3 and Table 3.4.

Table 3.3 Properties of Ethylene Glycol

Solvent	Acidity	Chloride	Iron	Water	Specific Gravity at 25 C	Viscosity (@ 25 oC)	Manufacturer
Ethylene Glycol	27 ppm	<1 ppm	< 100 ppm	210 ppm	1.113	0.01663 Pa-s	Mallinckrodt Chemicals

Table 3.4 Properties of DI Water

Solvent	Grade	SiO2	Organic Carbon	Phosphate	Nitrate	Sulfate	Viscosity (@ 25 °C)	Manufacturer
DI Water	Reagent	< 3 ppb	< 100 ppb	< 1 ppm	< 0.2 ppm	< 1 ppm	9.04 x10-4 Pa-s	Ricca Chemical Company

4.0 RESULTS AND DISCUSSION

This chapter discusses the thermal conductivity enhancement of nanofluids over those of the base fluids alone. The nanofluid samples were sonicated in an ultrasonic cleaner before thermal conductivity measurements. The results obtained from DI water-based nanofluids are presented first, followed by the discussion of ethylene glycol-based nanofluids. Finally, the effect of using a different sonicating technique (e.g. sonicating probe) on the thermal conductivity enhancement of nanofluids is discussed.

4.1 Thermal Conductivity Enhancement of DI Water-Based Nanofluids

Figure 4.1 shows the dependence of thermal conductivity enhancement on the particle volume fraction for aluminum oxide-DI water nanofluids. The thermal conductivity enhancement is calculated from the following formula:

$$\text{Thermal Conductivity Enhancement}(\%) = \left(\frac{\lambda_{nanofluid}}{\lambda_{base}} - 1\right) x100 \qquad (4.1)$$

where $\lambda_{nanofluid}$ is the thermal conductivity of a nanofluid and k_{base} is the thermal conductivity of the base fluid

Predictions based on Maxwell-Garnett model with and without boundary thermal resistance are also shown to compare the experimental results with the model. Results show that the thermal conductivity enhancement increases with the volume fraction of aluminum oxide nanoparticles (see Figure 4.1). The trend in the absolute value of thermal conductivity enhancement follows from those normalized by the thermal conductivity of base fluids (see

Figure 4.1(a) and (b)). As seen in Figure 4.1(a), the highest thermal conductivity enhancement observed in the current experiment is 16% at a particle volume fraction of ~8%. Also, results show that at a given particle volume fraction, the difference in the thermal conductivity enhancement between the current data and the data obtained from Lee is within 2%. This is expected because both the current sample and Lee's sample are comparable in particle size, and both samples were prepared by a two-step method. Comparing the experiments to the model, Figure 4.1(a) shows that the current data agrees well with the Maxwell-Garnett model with the boundary thermal resistance, whereas the data obtained from Lee fall between the Maxwell-Garnett model with and without the boundary thermal resistance [2]. Cahill and co-worker measured boundary thermal resistance between platinum nanoparticles (10 nm in diameter) and water to be 7.7×10^{-9} Km^2W^{-1} [34], which is used as an approximation for the boundary thermal resistance between aluminum oxide nanoparticles (47 nm) and water in the current sample due to the similarity in particle size.

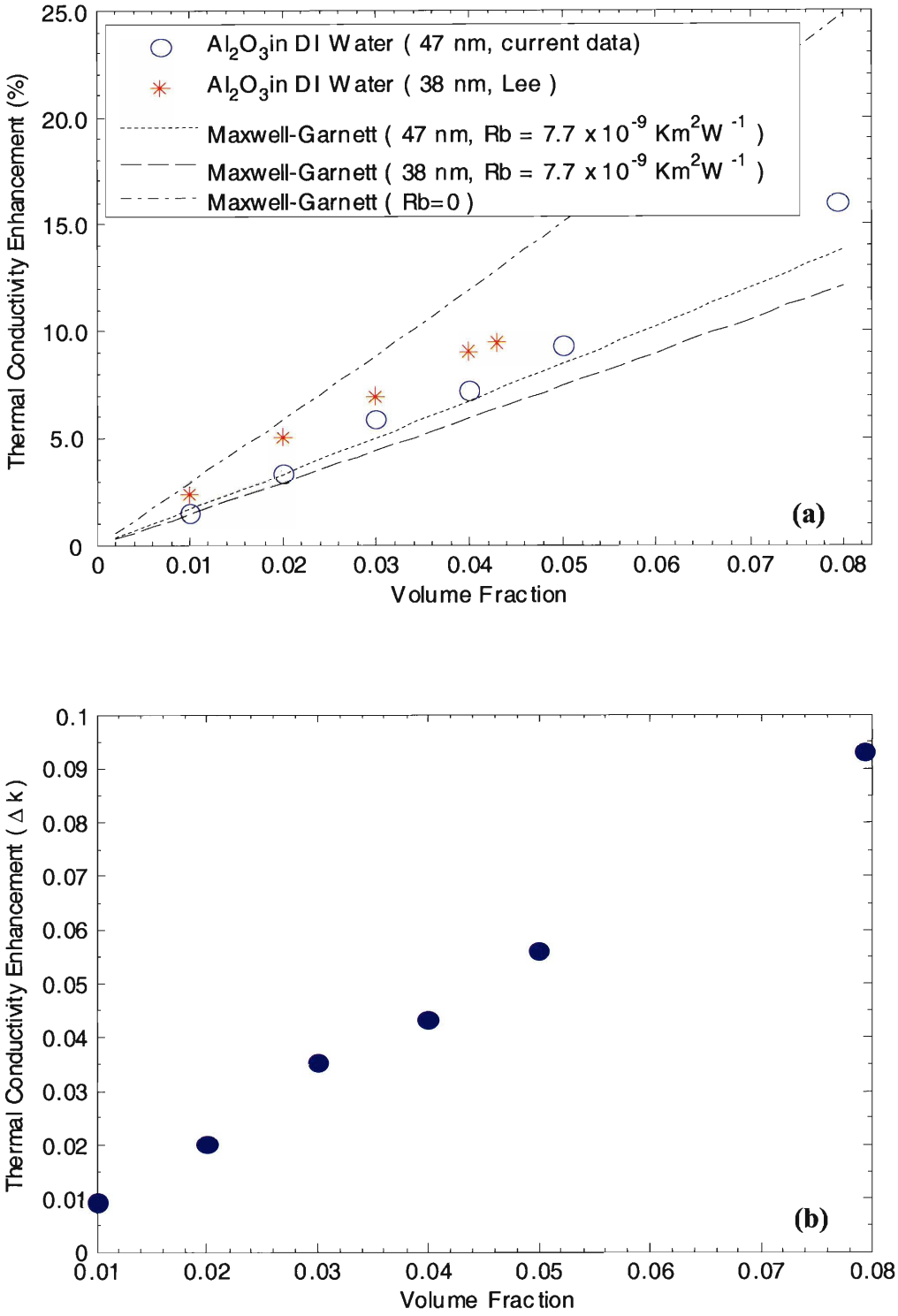

Figure 4.1 (a) Thermal Conductivity Enhancement (%) of Aluminum Oxide-DI Water Nanofluids (b) Thermal Conductivity Enhancement (Δk) of Aluminum Oxide-DI Water Nanofluids

Figure 4.2 shows the thermal conductivity enhancement of gold-DI water nanofluids with particle diameter of 5, 15, and 30 nm. Each sample has the same particle volume concentration of ~0.27%. As illustrated in Figure 4.2, no thermal conductivity enhancement is observed for samples both with and without surfactant. This result can be attributed to the low particle concentrations in these samples. Low particle concentration results in long inter-particle distance and large regions of particle-free liquid with high thermal resistance [7]. The observed thermal conductivity enhancement for all the samples follows from the Maxwell-Garnett predictions (see Figure 4.2).

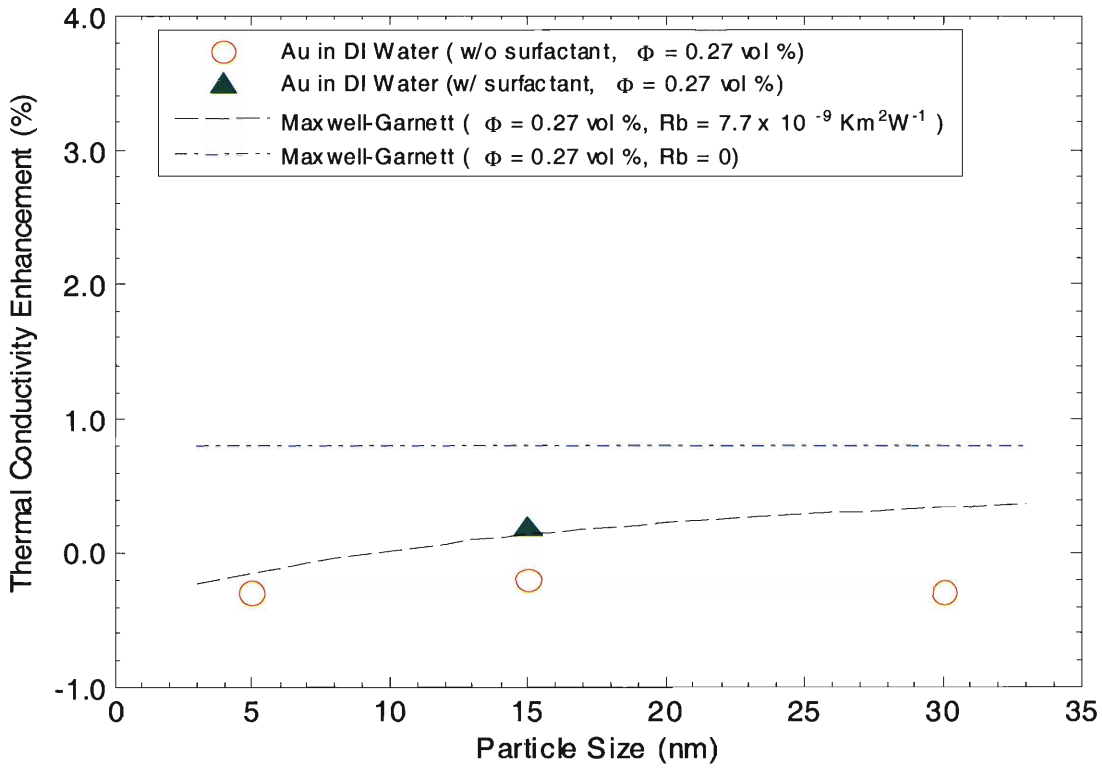

Figure 4.2 Thermal Conductivity Enhancement of Gold-DI Water Nanofluids

4.2 Thermal Conductivity Enhancement of Ethylene Glycol-Based Nanofluids

The relationship between the thermal conductivity enhancement and the particle volume fraction for aluminum oxide-ethylene glycol nanofluids is depicted in Figure 4.3. As shown in this figure, the thermal conductivity enhancement increases linearly with particle volume fraction. The trend in the absolute value of thermal conductivity enhancement follows from those normalized by the thermal conductivity of base fluids (see Figure 4.3(a) and (b)). Figure 4.3(a) shows that thermal conductivity of the current sample can be enhanced by ~15% at particle volume fraction of ~5%. At the same particle volume fraction, dispersion of aluminum oxide in DI water results in only ~9% enhancement in thermal conductivity (see Figure 4.1(a)). This indicates that aluminum oxide nanoparticles are more effective in improving the thermal transport property when they are dispersed in ethylene glycol than in DI water. As illustrated in Figure 4.3(a), the current data fall along the Maxwell-Garnett prediction without the boundary thermal resistance.

By comparing results obtained from different research groups, Figure 4.3(a) shows that at relatively low particle volume fraction, the current data agrees well with the data obtained from Lee and Eastman [2, 6]. However, the observed thermal conductivity enhancement among different groups diverges at relatively high particle volume fraction. It has been found that rapid clustering of nanoparticles occurs at high particle concentration, and the thermal conductivity enhancement of nanofluids is directly related to the clustering of nanoparticles [35]. Thus, the difference in the size and structure of agglomerates among different nanofluid samples can possibly explain the divergence of experimental data at relatively high particle concentration.

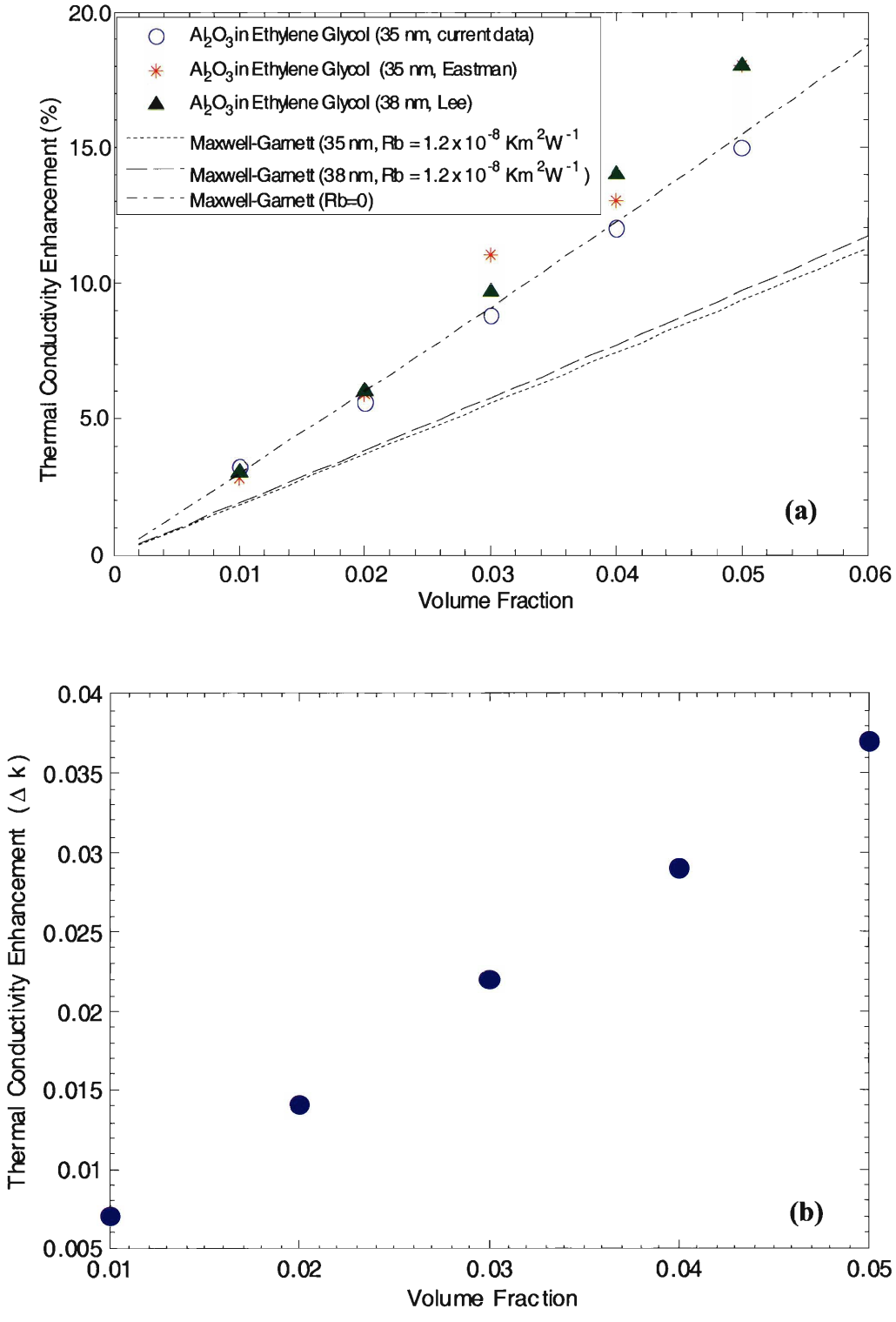

Figure 4.3 (a) Thermal Conductivity Enhancement (%) of Aluminum Oxide-Ethylene Glycol Nanofluids (b) Thermal Conductivity Enhancement (Δk) of Aluminum Oxide-Ethylene Glycol Nanofluids

Figure 4.4 shows the thermal conductivity enhancement for the gold-ethylene glycol nanofluids with different particle diameters. These nanofluid samples contain the same volume fraction of gold nanoparticles (~0.3%). As shown in Figure 4.4, for the samples without surfactant the thermal conductivity enhancement is relatively constant at ~6% at particle diameter of 5, 15, and 30 nm. This indicates that the enhancement in thermal conductivity is not dependent on the size of the gold nanoparticles prior to their dispersion in ethylene glycol. For the sample with surfactant, the observed thermal conductivity enhancement is ~12%, which is higher than those without surfactant by nearly a factor of two. Calculations based on Maxwell-Garnett model show a less than ~1% enhancement in thermal conductivity. Later material analysis of these gold-ethylene glycol nanofluids by ATR-FTIR technique suggests that the observed analomous enhancement can be due to the presence of water (see Section 4.4).

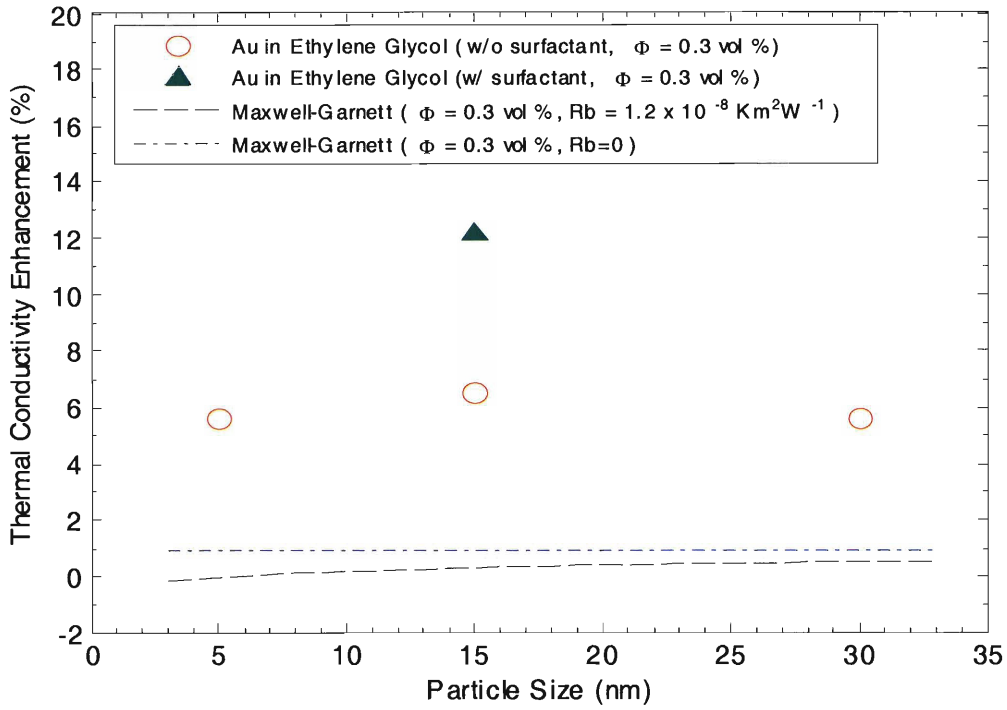

Figure 4.4 Thermal Conductivity Enhancement of Gold-Ethylene Glycol Nanofluids

4.3 Thermal Conductivity Enhancement of Gold-Ethylene Glycol Nanofluids

In view of the significant thermal conductivity enhancement observed with the gold-ethylene glycol nanofluids, a systematic dilution was performed to study its behavior at lower particle concentration. Figure 4.5 plots the dependence of thermal conductivity enhancement on the particle volume concentration for the sample with particle diameter of 15 nm and with surfactant. Similar plot for the sample with particle diameter of 30 nm and without surfactant are shown in Figure 4.6. These two figures indicate that the thermal conductivity enhancement for both gold nanofluid samples decreases linearly as the nanofluids were diluted to lower particle concentration. Even at the lowest particle concentration, the observed thermal conductivity enhancement is higher than Maxwell-Garnett prediction by a significant amount.

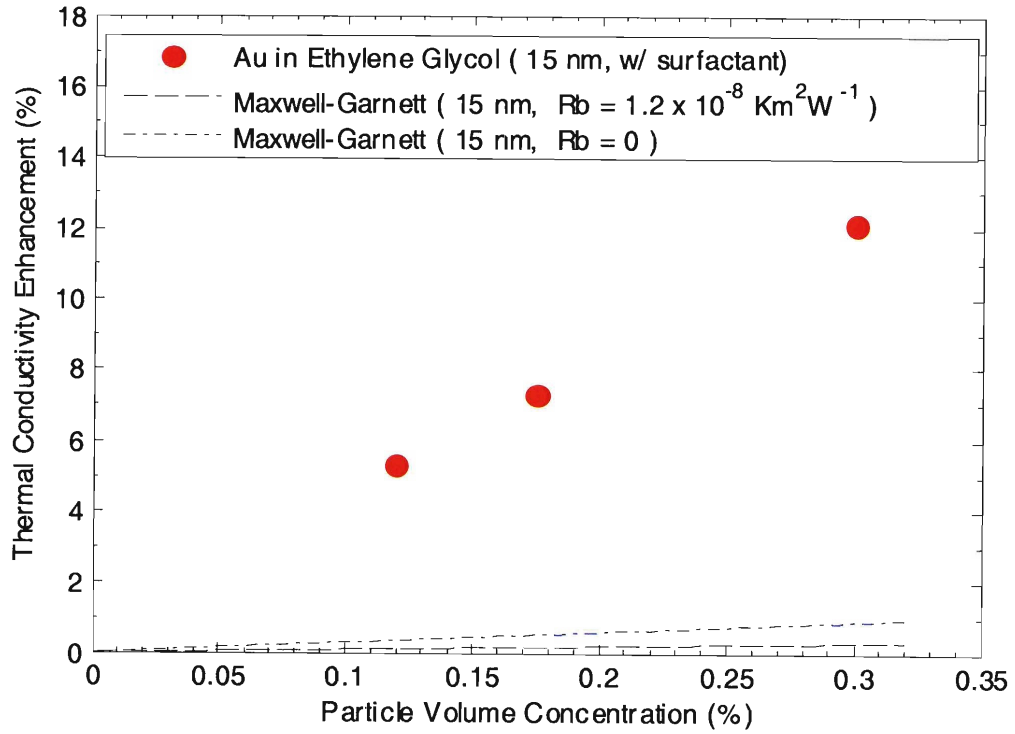

Figure 4.5 Thermal Conductivity Enhancement of Gold-Ethylene Glycol Nanofluid with Particle Diameter of 15 nm, with Surfactant

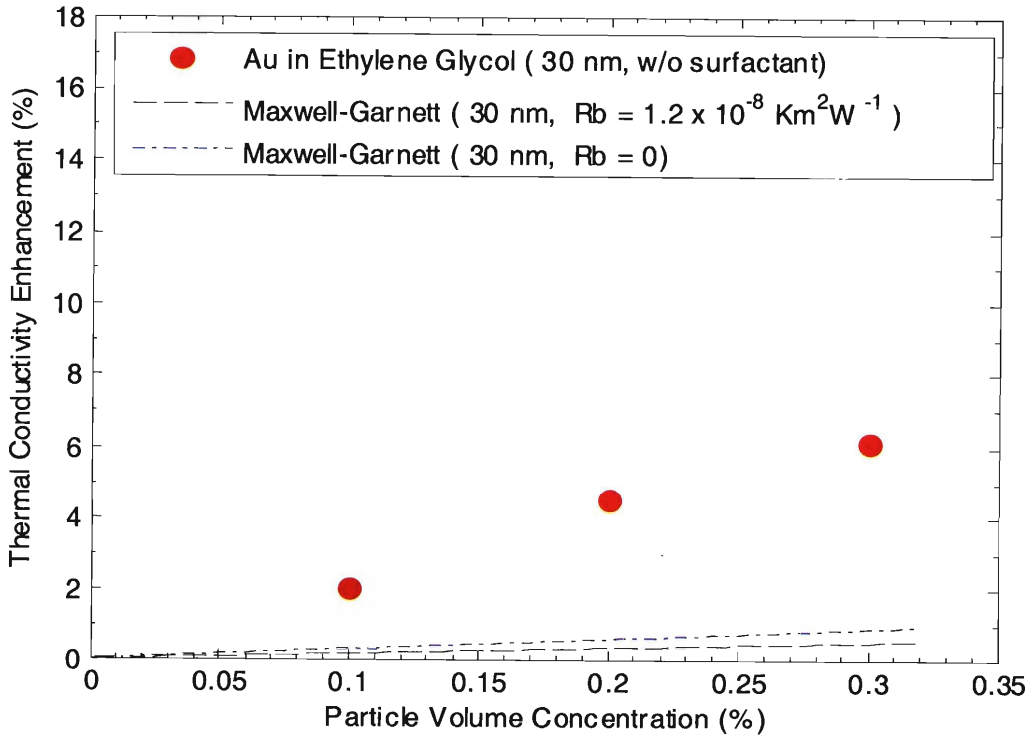

Figure 4.6 Thermal Conductivity Enhancement of Gold-Ethylene Glycol Nanofluid with Particle Diameter of 30 nm, without Surfactant

As discussed in Section 3.2, the thermal conductivity enhancement is higher when the gold nanoparticles are dispersed in ethylene glycol than in DI water. Hence, it is of interest to see the enhancement in thermal conductivity when the gold nanoparticles are dispersed in ethylene glycol and water mixture. The resulting nanofluid mixture of gold, DI water and ethylene glycol was prepared by adding DI water into a gold-ethylene glycol nanofluid sample with particle diameter of 5 nm and particle volume concentration of ~0.3%. As more water was added to the nanofluid mixture, the particle volume concentration decreases as a consequence (see Figure 4.7).

The effect of DI water volume concentration on the thermal conductivity of the nanofluid mixture is shown in Figure 4.8. This figure also shows the thermal conductivity of DI water and ethylene glycol mixture as a function of DI water volume concentration, which is used as a baseline thermal conductivity with which the thermal conductivity of the nanofluid mixture is compared. As seen in Figure 4.8, at a given volume concentration of DI water, the thermal conductivity of the nanofluid mixture is higher than that of DI water and ethylene glycol mixture. This is attributable to the presence of gold nanoparticles in the nanofluid mixture.

Figure 4.9 plots the thermal conductivity enhancement of the nanofluid mixture over the baseline thermal conductivity as a function of DI water volume concentration in the nanofluid mixture. This figure shows that between 0 and 35 vol. % of DI water in the nanofluid mixture, the thermal conductivity enhancement increases with the increased DI water volume concentration even though the gold particle volume concentration decreases due to the addition of water (see Figure 4.9). This suggests that in this regime, the relative proportion of ethylene glycol and DI water in the nanofluid mixture has more significant

effect on the thermal conductivity enhancement than the gold particle concentration. The decreasing trend after the maximum enhancement in thermal conductivity at DI water volume concentration of ~35% can be possibly due to the fact that as the concentration of gold nanoparticle drops below a critical point, the thermal conductivity enhancement starts to fall with increasing DI water volume concentration. The observed thermal conductivity enhancement of the nanofluid mixture is significantly higher than that predicted by the Maxwell-Garnett theory (see Figure 4.9).

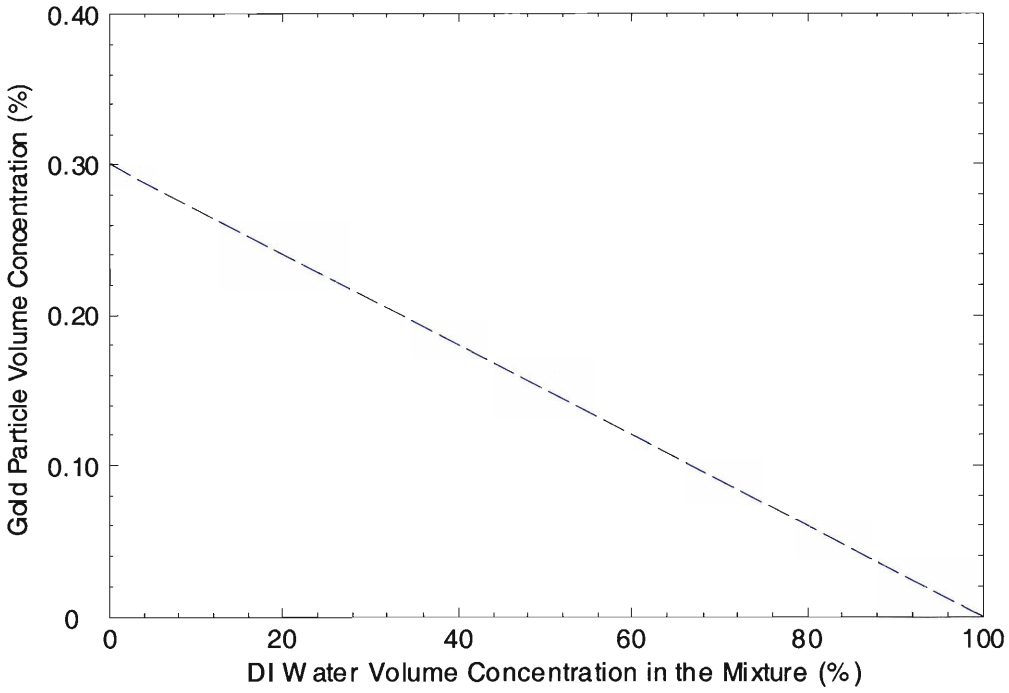

Figure 4.7 Gold Particle Volume Concentration as a Function of DI Water Volume Concentration in the Mixture

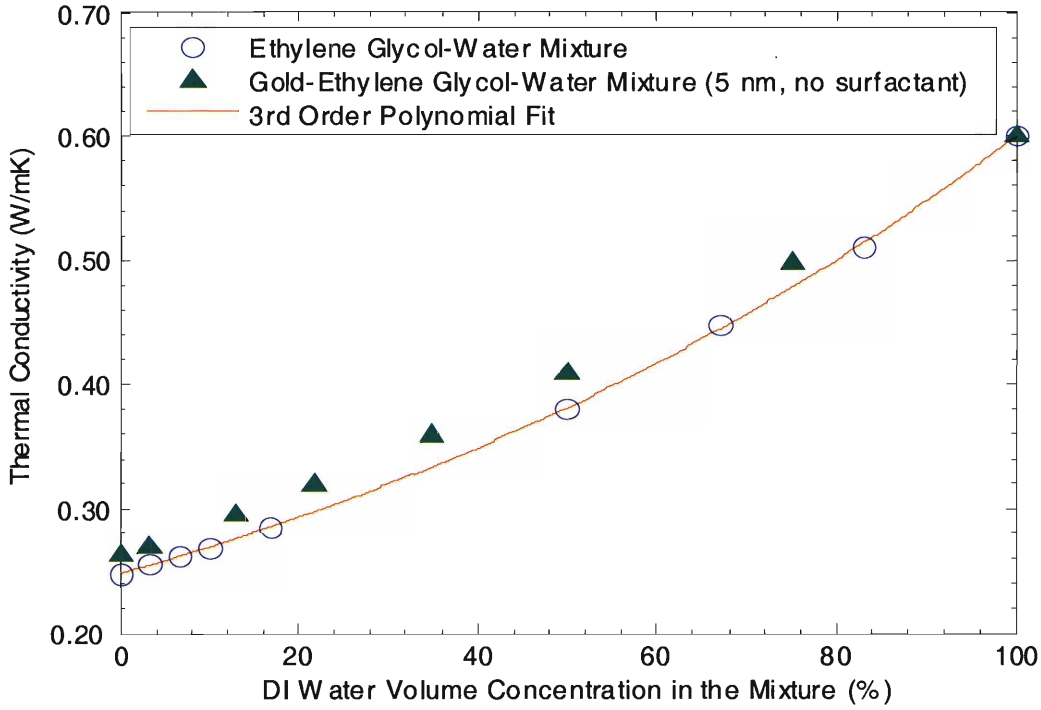

Figure 4.8 Thermal Conductivity of Gold, Ethylene Glycol, and DI Water Mixture as a Function of DI Water Volume Concentration

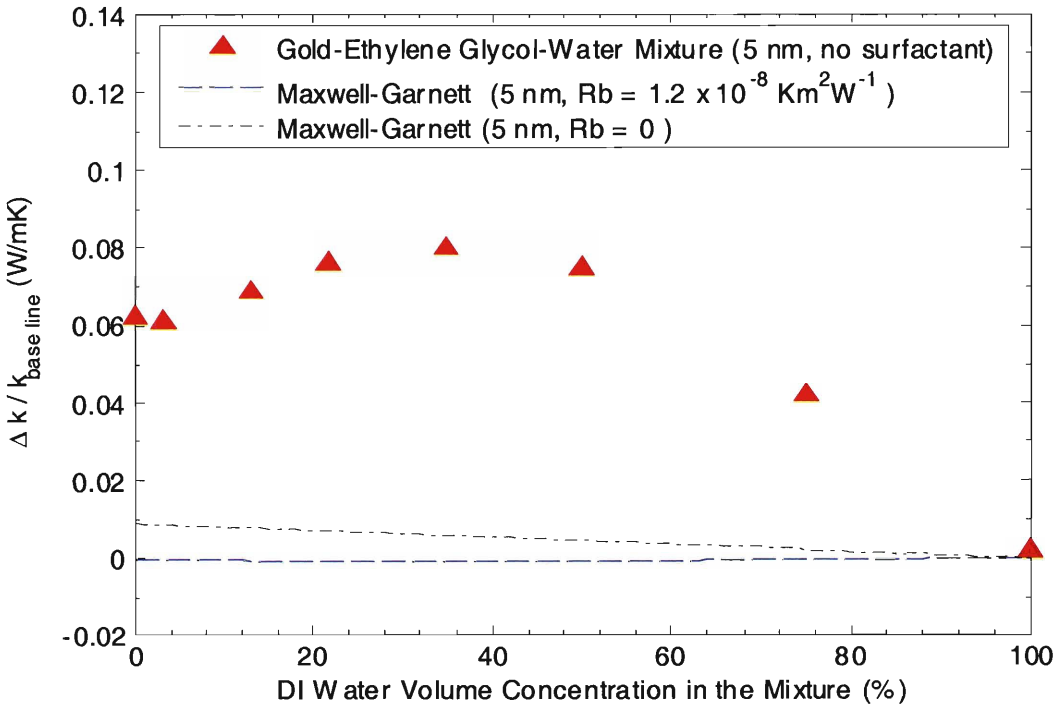

Figure 4.9 Thermal Conductivity Enhancement of Gold, Ethylene Glycol, and DI Water Mixture as a Function of DI Water Volume Concentration

4.4 ATR-FTIR Analysis of the Gold-Ethylene Glycol Nanofluid

It was assumed that the anomalous enhancement in thermal conductivity observed from the gold-ethylene glycol nanofluids may be attributable to the presence of water. This assumption was made based on the following reasons. First, viscosity measurements by Professor McKinley's Group on the gold-ethylene glycol nanofluids showed reducing viscosity with the increased particle volume fraction. Also, data indicates that thermal conductivity of ethylene glycol increases as ethylene glycol is exposed to atmosphere for extended period of time (see Table 4.1), which is possibly due to water absorption. Finally, details of manufacturing processes for the nanofluid samples are unclear. Hence, ATR-FTIR analysis was performed on the gold-ethylene glycol nanofluid sample with particle diameter of 30 nm and without surfactant to see whether there is presence of water in the sample.

Figure 4.10 shows the ATR absorption spectra for the gold nanofluid sample plotted against those for ethylene glycol and DI water. The peaks observed at the wavenumber of ~3750 cm^{-1} are due to the background noise collected by the ATR crystal. As seen in Figure 4.10, spectrum of the nanofluid sample generally follows from ethylene glycol. However, as opposed to total transmittance shown in the spectrum of ethylene glycol at ~1650 cm^{-1}, a small absorption (shown as a small bump) is shown in the spectrum of the nanofluid sample at the same wavenumber. A comparison between spectra of the nanofluid sample and DI water suggests that this bump may indicate the presence of small amount water in the nanofluid sample.

Table 4.1 The Effect of Atmospheric Exposure on the Thermal Conductivity of Ethylene Glycol

Days of Atmospheric Exposure	0	12	33
Measured Thermal Conductivity (W/mK)	0.247	0.252	0.257
Thermal Conductivity Enhancement (%)	0	2.0	4.0

To estimate the amount of water in the nanofluid sample, ATR spectra were collected for ethylene glycol and DI water mixtures with different water volume concentrations, and the results were plotted against the spectrum of the gold nanofluid sample (see Figure 4.11). A zoom-in of the absorption peaks at ~1650 cm^{-1} was inserted as an inset of Figure 4.11. As shown in Figure 4.11, the absorption peak of ethylene and water mixture at ~1650 cm^{-1} rises with the increased water volume concentration. The height and area of this peak at ~1650cm^{-1} for the mixture with water volume concentration of ~6.7% are similar to those for the gold nanofluid sample (see inset of Figure 4.11). This suggests that the gold nanofluid sample may contain ~6.7 vol. % of water, which caused the observed anomalous enhancement in thermal conductivity.

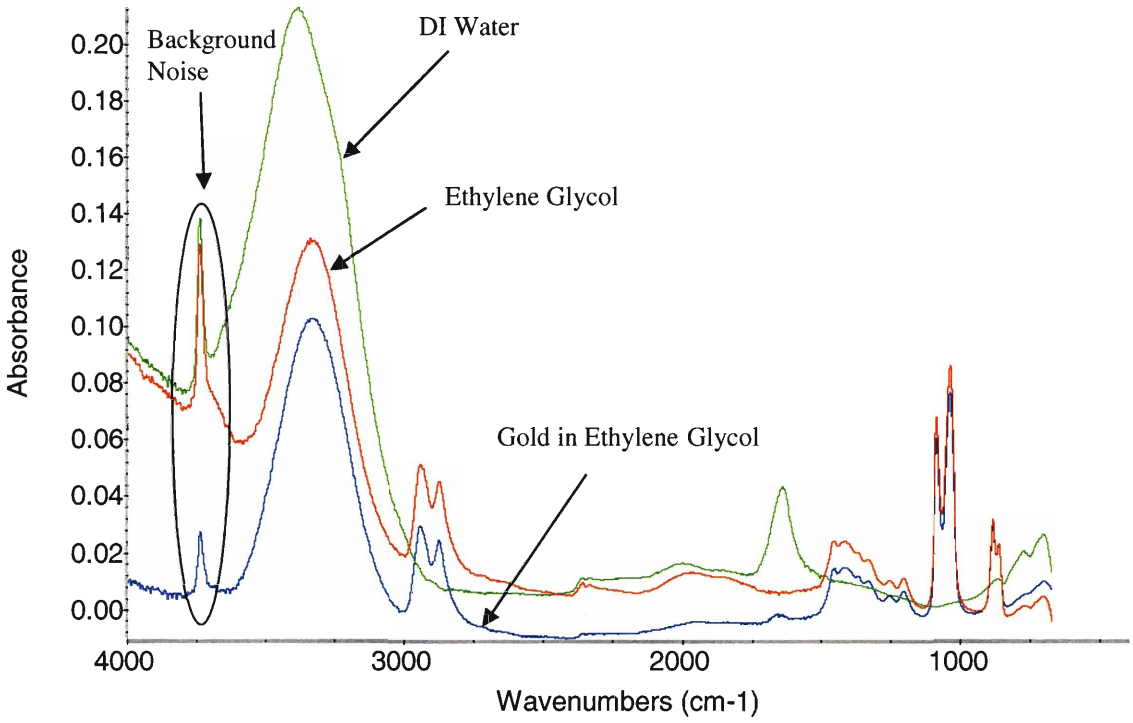

Figure 4.10 ATR Absorption Spectra for Gold in Ethylene Glycol Nanofluid, Ethylene Glycol, and DI Water. The peaks at ~3750 cm^{-1} are due to the noises collected by the ATR crystal.

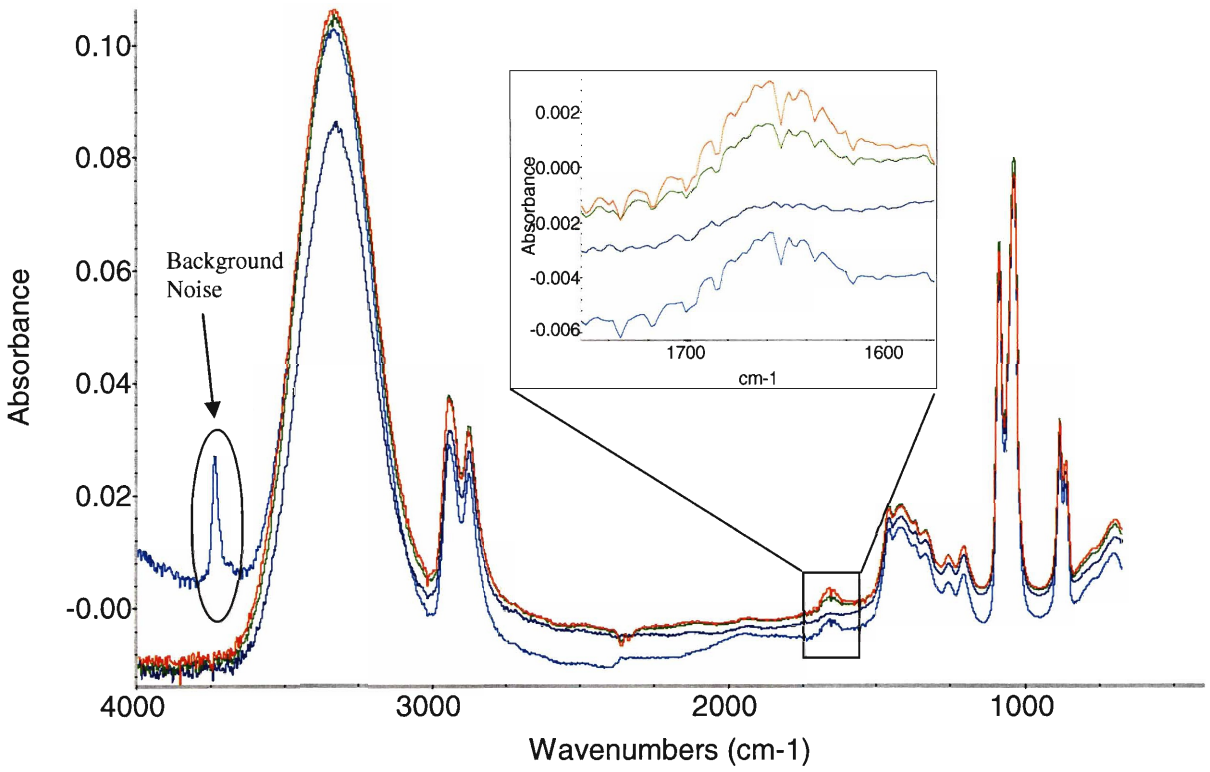

Figure 4.11 ATR Absorption Spectra for Gold in Ethylene Glycol Nanofluid, and Mixtures of Ethylene Glycol and DI Water. A zoom-in of the absorption peaks at ~1650 cm^{-1} is shown as an inset. The spectra are color-coded. Blue: gold-ethylene glycol nanofluid; Black: 3.3 vol. % DI water in ethylene-glycol; Green: 6.7 vol. % DI water in ethylene glycol; Red: 10 vol. % DI water in ethylene glycol

4.5 The Effect of Different Sonicating Techniques on the Thermal Conductivity Enhancement of Nanofluids

Thermal conductivity enhancement as a function of particle volume fraction for the aluminum oxide-DI water nanofluid (47 nm) was obtained after sonicating the sample by an ultrasonic probe, and the results were plotted against those obtained after sonicating in an ultrasonic cleaner (see Figure 4.12). The total amount of energy delivered to the sample was held constant at ~16000 J for both sonicating techniques, but the rate at which this ultrasonic energy delivered was much faster with the sonicating probe (750 J/s) than with the ultrasonic cleaner (70 J/s). As shown in Figure 4.12, at the same particle volume fraction, the observed thermal conductivity enhancement is higher with the sonicating probe technique than with the ultrasonic cleaner technique. The difference in thermal conductivity enhancement between different sonicating techniques increases with the increased particle volume fraction, and is as large as ~10% at particle volume fraction of ~8%. This trend is possibly attributable to the rapid particle clustering at high volume fraction, so a more powerful sonicating tool is required to break large agglomerates into smaller constituents.

Figure 4.12 also shows that the thermal conductivity enhancement obtained with the sonicating probe technique falls along the Maxwell-Garnett model without the boundary thermal resistance. According to the Maxwell-Garnett model, the thermal conductivity enhancement of a particle-liquid mixture decreases with decreased particle size due to larger contribution of boundary thermal resistance in the overall resistance to heat flow. However, an opposite trend is seen in the experimental results, as the observed thermal conductivity enhancement increases with a decrease in particle size. The discrepancy between the model and the experiment suggests that there exist other heat transfer mechanisms beyond those considered in the model [18, 20].

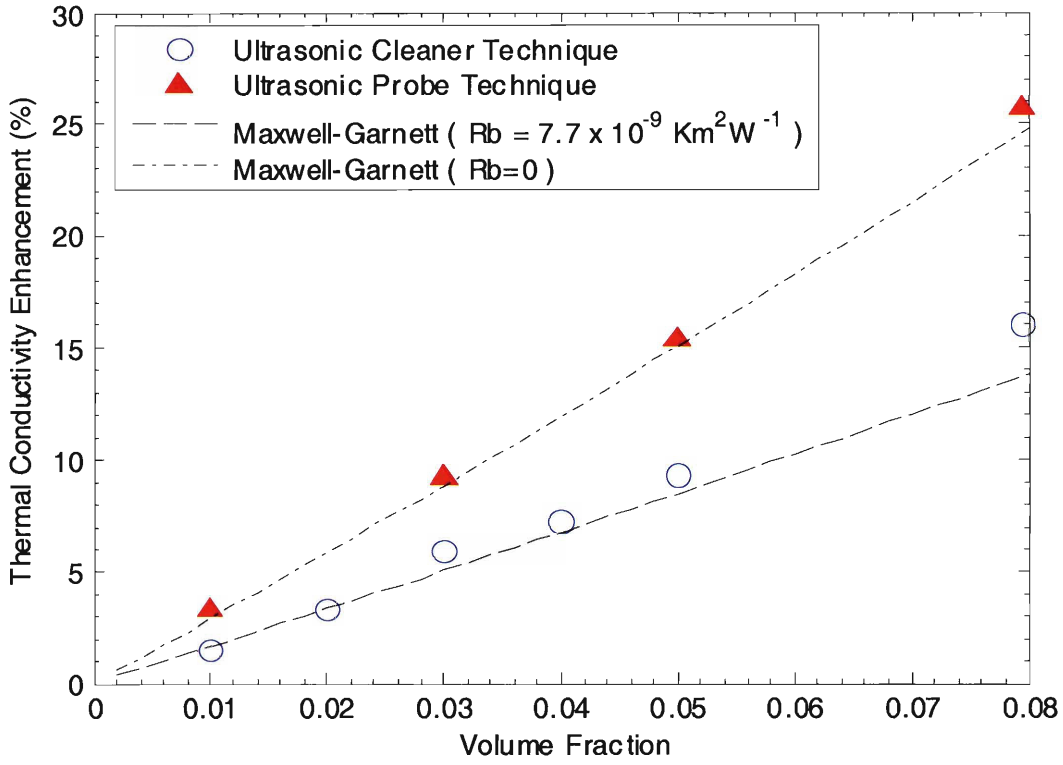

Figure 4.12 The Effect of Different Sonicating Techniques on the Thermal Conductivity Enhancement of Aluminum Oxide in DI Water Nanofluid.

Chapter 5: Conclusion and Future Work

Transient hotwire technique was used to measure the thermal conductivity of DI water- and ethylene glycol-based nanofluids containing dispersion of aluminum oxide and gold nanoparticles. Results show that nanofluids, except for the ones with gold nanoparticles in DI water, exhibit higher thermal conductivity than their respective base fluids, and the thermal conductivity enhancement increases with the increased volume concentration of nanoparticles. Comparing the results of DI water-based nanofluids with those of ethylene glycol-based nanofluids, it can be seen that the thermal conductivity enhancement is higher when the nanoparticles are dispersed in ethylene glycol than in DI water.

The current sample of aluminum oxide in DI water exhibits an enhancement in thermal conductivity by ~16% at the particle volume fraction of ~8%. For the aluminum oxide-ethylene glycol sample, ~15% enhancement in thermal conductivity is observed at particle volume fraction of ~5%. The observed thermal conductivity enhancement of these aluminum oxide nanofluid samples is comparable to the Maxwell-Garnett approximations.

The enhancement in thermal conductivity for nanofluids containing gold nanoparticles is found to be strongly dependent on the base fluid. For the gold in DI water nanofluids, no thermal conductivity enhancement is observed. However, dispersion of gold nanoparticles in ethylene glycol without the use of surfactant shows ~6% enhancement in thermal conductivity at particle volume concentration of only ~0.3%. This thermal conductivity enhancement is found to be independent with the size of the gold nanoparticles prior to their dispersion in ethylene glycol. At the same volume concentration of gold nanoparticles in ethylene glycol (~0.3%), results show that the thermal conductivity enhancement can be raised to ~12% with the aid of surfactant (Pyridine). However, calculation based on Maxwell-Garnett model

predicts a thermal conductivity enhancement of only less than ~1% for these gold-ethylene glycol nanofluids. ATR-FTIR analysis suggests that this large discrepancy between the model and the experiment may be attributable to the presence of water in the gold-ethylene glycol nanofluids.

Investigation of the effect of different sonicating techniques on the thermal conductivity enhancement of aluminum oxide-DI water nanofluid indicates that the enhancement in thermal conductivity is dependent on the strength of the sonicating tool. As compared to the ultrasonic cleaner (70W), the use of a more powerful sonicating probe (750W) results in a higher thermal conductivity enhancement. The beneficial effect of using sonicating probe on the thermal conductivity enhancement of aluminum oxide-DI water nanofluid is more pronounced at high particle volume fraction. At particle volume fraction of ~8%, the enhancement in thermal conductivity is ~26% with the use of a sonicating probe, whereas only ~16% enhancement in thermal conductivity was observed after sonicating the sample in an ultrasonic cleaner.

The thermal conductivity data obtained from different sonicating techniques is very interesting, and further systematic studies are needed to understand the discrepancy in thermal conductivity enhancement between different sonicating techniques. One approach is to investigate the agglomerated size and structure of nanoparticles in nanofluids. Traditional characterization technique such as transmission electron microscopy (TEM) cannot image the nanoparticles in suspension. Hence, a new experimental technique needs to be developed to *in-situ* characterize the size and distribution of aggregates in nanofluids.

BIBLIOGRAPHY

[1] H. Masuda, A. Ebata, K. Teramae, N. Hishinuma, "Alteration of Thermal Conductivity and Viscosity of Liquid by Dispersing Ultra-Fine Particles," *Netsu Bussei* Vol **4**, 1993, pp. 227-33

[2] S. Lee, S. U. S. Choi, S. Li, and J. A. Eastman, "Measuring Thermal Conductivity of Fluids Containing Oxide Nanoparticles," *Journal of Heat Transfer*, Vol. **121**, 1999, pp. 280-289

[3] H. Xie, J. Wang, T. Xi, Y. Liu, and F. Ai, "Thermal conductivity enhancement of suspensions containing nanosized alumina particles," *Journal of Applied Physics*, Vol **91**, No 7, 2002, pp. 4568-4572.

[4] S. Das, N. Putra, P. Thiesen, and W. Roetzel, "Temperature Dependence of Thermal Conductivity Enhancement for Nanofluids," *Journal of Heat Transfer*, Vol. **125**, 2003, pp. 567-574.

[5] M. Liu, M. Lin, I. Huang, C. Wang, "Enhancement of thermal conductivity with carbon nanotube for nanofluids," *International Communication in Heat and Mass Transfer*," Vol **32**, 2005, pp. 1202-1210

[6] J.A. Eastman, S.U. S. Choi, S. Li, W. Yu, L. J. Thompson, "Anomalously increased effective thermal conductivities of ethylene glycol-based nanofluids containing copper nanoparticles," *Appl. Phys. Lett.*, Vol **78**, 2001, pp.718-20

[7] J. A. Eastman, S. R. Phillpot, S. U. S. Choi, P. Keblinski, "Thermal Transport in Nanofluids," *Annu. Rev. Mater. Res.*, Vol. **34**, 2004, pp. 219-246

[8] C.W. Sohn and M. M. Chen, "Microconvective thermal conductivity in disperse two phase mixture as observed in a low velocity Couette flow experiment," *Journal of Heat Transfer, Trans. ASME*, Vol **103,** 1981, pp. 47-51

[9] A. S. Ahuja, "Augmentation of heat transport in laminar flow of polystyrene suspension," *Journal of Applied Physics*, Vol **46**, 1975, pp 3408-3425

[10] G. Hetsroni and R. Rozenblit, "Heat transfer to a liquid-solid mixture in a fume," *International Journal of Multiphase Flow*," Vol. **20**, 1994, pp. 671-689

[11] C.G. Granqvist and R. A. Buhrman, "Ultra-fine metal particles," *Journal of Applied Physics*, 1976, 47:2200

[12] S. Yatsuya, Y. Tsukasaki, K. Mihama, and R. Uyeda, "Preparation of extremely fine particles by vacuum evaporation onto a running oil substrate," *Journal of Crystalline Growth*, 1978, 45:490

[13] V. V. Srdic, M. Winterer, A. Moller, G. Miehe, and H. Hahn, "Nanocrystalline zirconia surface-doped with alumina: chemical vapor synthesis, characterization, and properties," *Journal of American Ceramic Society*, 2001, Vol. 84, pp. 2771-2776

[14] H. Gleiter, "Theory of grain boundary migration rate,"*Acta Metallurgica*, 1969, Vol **17**, No. 7, pp. 853-862.

[15] S. Behrens, H. Bonnemann, N. Matoussevitch. E. Dinjus., H. Modrow, N. Palina, M. Frerichs, V. Kempter, W. Maus-Friedrichs., Heinemann, A, M. Kammel, A. Wiedenmann, L. Pop, S. Odenbach, E. Uhlmann, N. Bayat, J. Hesselbach, J.M. Guldbakke, "Air-stable Co-, Fe-, and Fe/Co-nanoparticles and ferrofluids," *Zeitschrift fur Physikalische Chemie*, Vol. **220**, No. 1, 2006, p 3-40

[16] L. P. Zhou, B. X. Wang, "Experimental Research on the Thermophysical Properties of Nanoparticle Suspension Using the Quasi-Steady Method," *Annu. Proc. Chin., Eng. Thermophys.*, 2002, pp. 889-892.

[17] H.E. Patel, S. K. Das, T. Sundararajan, A. S. Nair, B. Georage, T. Pradeep, "Thermal conductivities of naked and monolayer protected metal nanoparticle based nanofluids: Manifestation of anomalous enhancement and chemical effects, *Appl. Phys. Lett.*, Vol **83**, pp. 2931-2933

[18] J. C. Maxwell, "A Treatise on Electricity and Magnetism," 3rd edition, (Dover, New York, 1954), Vol **1**, p. 435.

[19] F. Incropera and D. DeWitt, "Fundamentals of Heat and Mass Transfer," *John Wiley & Sons*, Inc, 2001, pp. 93-95

[20] D. P. H. Hasselman and L. F. Jphnson, "Effective Thermal Conductivity of Composites with Interfacial Thermal Barrier Resistance," *Journal of Composite Materials*, Vol **21**, 1987, pp. 508-515

[21] L. Xue and P. Keblinski, S.R. Phillpot, S.U.-S. Choi, and J. A. Eastman, "Two regimes of thermal resistance at a liquid-solid interface," *Journal of Chemical Physics*, Vol **118**, No. 1, 2003, pp. 337-339

[22] H. Hatta and M. Taya, "Thermal Conductivity of Coated Filler-Composites," *Journal of Applied Physics*, 1986, 59:1851

[23] B. R. Powell, G.E. Youngblood, D. P. H. Hasselman, and L.D. Bentsen, "Effect of Thermal Expansion Mismatch on the Thermal Diffusivity of Glass-Ni Composites," *Journal of American Ceramic Society*, 1980, 63:581.

[24] L. Xue, P. Keblinski, S. R. Phillpot, S. U. S. Choi, and J. A. Eastman, "Effect of liquid layering at the liquid-solid interface on thermal transport," *International Journal of Heat and Mass Transfer*, 2004.

[25] P. Keblinski, S.R. Phillpot, S. U. S. Choi, and J. A. Eastman, "Mechanisms of heat flow in suspensions of nano-sized particles (nanofluid)," *International Journal of Heat and Mass Transfer*, Vol **45**, 2002, pp. 855-863

[26] B. X. Wang, P. P. Zhou, Z. F. Peng, "A fractal model for predicting the effective thermal conductivity of liquid with suspension of nanoparticles," *International Journal of Heat and Mass Transfer*, Vol **46**, 2003, pp. 2665-2672

[27] A. R. Challoner and R. W. Powell, "Thermal Conductivities of Liquids: New Determinations for Seven Liquids and Appraisal of Existing Values," *Proceedings of Royal Society of London. Series A*, Vol. **238**, No. 1212, 1956, pp. 90-106

[28] X. Wang and X. Xu, "Thermal Conductivity of Nanoparticle-Fluid Mixture," *Journal of Thermophysics and Heat Transfer*, Vol. **13**, 1999, pp. 474-480

[29] Y. Nagasaka and A. Nagashima, "Absolute measurement of the thermal conductivity of electrically conducting liquids by the transient hot-wire-method," *J. Physs. E: Dci. Instrum*, Vol. **14**, 1981, pp. 1435-1440

[30] C. Castro, J. Calado, W. A. Wakeham, and M. Dix, "An Apparatus to measure the thermal conductivity of liquids," *Journal of Physics E: Science Instrument*, Vol. **9**, 1976, pp. 1073-1080

[31] T. Beckwith, R. Marsngoni, and J. Lienhard, "Mechanical Measurements," 5th edition, *Addison-Wesley Publishing Company, Inc*, 1995, pp. 668-676.

[32] S. N. Rasuli and R. Golestanian, "Thermophoresis for a single charged colloidal particle," *Journal of Physics: Condensed Matter*, Vol. **17**, No. 14, 2005, pp. S1171-6

[33] H. Ohshima, "Electrophoresis pf colloidal particles in a salt-free medium," *Chemical Engineer Scienc,* Vol. **61**, No. 7, 2006, pp. 2104-2107.

[34] O. M. Wilson, X. Hu, D. Cahill, and P. Braun, "Colloidal metal particles as probe of nanoscale thermal transport in fluids," *Physical Review B*, Vol. **66**, 2002, 224301

[35] K. S Hong, Tae-Keun Hong, and Ho-Soon Yang, "Thermal conductivity of Fe nanofluids depending on the cluster size of nanoparticles," *Applied Physics Letters*, Vol. **88**, 2006, 031901